

Eliminating leading and subleading corrections to scaling in the three-dimensional XY universality class

Martin Hasenbusch

*Institut für Theoretische Physik, Universität Heidelberg,
Philosophenweg 19, 69120 Heidelberg, Germany*

(Dated: July 28, 2025)

Abstract

We study the $(q + 1)$ -state clock model on the simple cubic lattice by using Monte Carlo simulations. In addition to the nearest neighbor coupling we consider a next-to-next-to-nearest neighbor coupling. For a certain range of the parameters, the phase transition of the model shares the XY universality class. Leading corrections to scaling are studied by using finite size scaling of dimensionless quantities, such as the Binder cumulant U_4 . The spatial unisotropy, which causes subleading corrections, is studied by computing the exponential correlation length ξ_{exp} in the high temperature phase for different directions. In the case of the q -state clock model it turns out that by tuning the ratio of the two coupling constants, we can eliminate either leading or subleading corrections to scaling. These points on the critical line are close to each other. Hence in the improved model, where leading corrections to scaling vanish, also subleading corrections are small. By using a finite size scaling analysis of our high statistics data we obtain $\eta = 0.03816(2)$ and $y_t = 1/\nu = 1.48872(5)$ as estimates of the critical exponents.

I. INTRODUCTION

We discuss the extension of the improved model programme, studying critical phenomena, to a two-parameter family of models at the example of the three-dimensional XY universality class. For reviews on critical phenomena see for example [1–5]. For a discussion of improved lattice models see in particular Sec. 2.3 of Ref. [5]. Studying critical phenomena by using Monte Carlo simulations of lattice models one might have different objectives. Either the model reproduces well the microscopic properties of the experimental system of concern or one is interested in properties of a universality class. In the latter case, we would like to obtain accurate estimates of universal quantities like critical exponents or amplitude ratios by simulating relatively small lattices, allowing for high statistics. To this end, the model should not be too complicated and one should be able to simulate it by using efficient algorithms such as the cluster algorithm [6, 7]. Here we study a model in the three-dimensional XY universality class, which fulfills these criteria. In Ref. [8] we studied the Blume-Capel model on the simple cubic lattice with nearest and next-to-next-to-nearest neighbor couplings. By tuning the ratio of the two coupling constants and the dynamic dilution parameter, also called crystal field, we were able to find a point in the parameter space, on the critical surface, where both the leading correction as well as the subleading correction, which is associated with the spatial unisotropy, are vanishing. In the case of the Ising universality class, the corresponding correction exponents are $\omega = 0.82968(23)$, and $\omega_{NR} = 2.022665(28)$, obtained by using the conformal bootstrap (CB) method [9, 10]. Note that these estimates are consistent with previous, less accurate estimates obtained by using Monte Carlo simulations and series expansions of lattice models or field theoretic methods. The finite size scaling (FSS) analysis of the Blume-Capel with nearest and next-to-next-to-nearest neighbor couplings results in the most accurate estimates of critical exponents by using Monte Carlo simulations of lattice models for the three-dimensional Ising universality class. The accuracy is clearly better than that of field-theoretic methods. It is only surpassed by the CB [9–12].

Here we study an analogous model with phase transitions in the XY universality class. To this end, the field variable $s_x \in \{-1, 0, 1\}$ is replaced by a two component vector, which has either unit length or vanishes. The precise definition of the model and a discussion of its phase diagram will be given below in sec. II. As already anticipated in the appendix of

Ref. [8], where preliminary work is reported, we do not find a point, where the amplitudes of both corrections exactly vanish. However there is a point in parameter space, where the amplitude of the leading correction vanishes and the spatial unisotropy is considerably reduced. This allows us to further improve the accuracy of critical exponents compared with Ref. [13]. Our estimates are fully compatible with those obtained by using the CB [14] and the error bars are of similar size. For recent reviews on the CB see for example [15, 16].

The three-dimensional XY universality class has attracted much attention, since the λ -transition of ^4He , which is well studied experimentally, is supposed to share this universality class. The most accurate result for the exponent α of the specific heat is obtained from an experiment under the condition of microgravity [17–19]: $\alpha = -0.0127(3)$, which corresponds to $\nu = (2 - \alpha)/d = 0.6709(1)$, exploiting the hyperscaling relation between the critical exponent of the correlation length ν and α . Field theoretic results at the time were considerably less accurate. See for example Ref. [20], where $\nu = 0.6703(15)$ and $0.6305(25)$ are obtained by using the $d = 3$ expansion and the ϵ -expansion, respectively.

Monte Carlo simulations in combination with the analysis of high temperature series of lattice models resulted in $\nu = 0.6717(1)$ [21], reaching the accuracy claimed by the experiment. This estimate was confirmed by more recent Monte Carlo simulations of lattice models, $\nu = 0.67183(18)$ [22] and $\nu = 0.67169(7)$ [13], and the estimate $\nu = 0.671754(99)$ obtained by using the CB [14]. There can be little doubt on the theoretical estimate of ν now, and it would be desirable to reanalyze the experimental results or even perform new ones. Our motivation for the present work is to further develop the concept of improved models and to provide accurate estimates of critical exponents as benchmark for other theoretical methods.

The outline of the paper is the following: In Sec. II we define the model and introduce the observables that are measured. In Sec. III we summarize results on corrections to scaling exponents given in the literature. Next in Sec. IV we analyze our data for the correlation length in the high temperature phase and compute the optimal ratio of the coupling constants. In Sec. V follows a FSS analysis of dimensionless quantities. We obtain accurate estimates of critical exponents. In Sec. VI we summarize our results and compare them with the literature.

II. THE MODEL

We consider the analogue of the Blume-Capel model with nearest neighbor and next-to-next-to-nearest neighbor interactions studied in Ref. [8]. We replace \mathbb{Z}_2 by \mathbb{Z}_q or, in the limit $q \rightarrow \infty$, by $O(2)$ symmetry. The model studied in Ref. [8] is defined by the reduced Hamiltonian

$$H = -K_1 \sum_{\langle xy \rangle} s_x s_y - K_3 \sum_{[xy]} s_x s_y + D \sum_x s_x^2 - h \sum_x s_x , \quad (1)$$

where the spin or field variable s_x might assume the values $s_x \in \{-1, 0, 1\}$ and $x = (x^{(0)}, x^{(1)}, x^{(2)})$ denotes a site on the simple cubic lattice, where $x^{(i)} \in \{0, 1, \dots, L_i - 1\}$. Furthermore, $\langle xy \rangle$ denotes a pair of nearest and $[xy]$ a pair of next-to-next-to-nearest, or third nearest (3N) neighbors on the lattice. In Ref. [8] the linear lattice size $L = L_0 = L_1 = L_2$ is equal in all three directions and periodic boundary conditions are employed.

The model defined below is more general than the one actually simulated and includes the model studied in Ref. [13] as special case. Here we are interested in the properties of the $O(2)$ -invariant fixed point. Finite values of q are taken for technical reasons: The simulation requires less CPU time and less memory. Note that for example in Refs. [23, 24] the 512-state clock model had been simulated as extremely good approximation of the XY model at the critical point. The reduced Hamiltonian is given by

$$\mathcal{H}_{q+1} = -K_1 \sum_{\langle xy \rangle} \vec{s}_x \cdot \vec{s}_y - K_3 \sum_{[xy]} \vec{s}_x \cdot \vec{s}_y - D \sum_x \vec{s}_x^2 - \vec{H} \cdot \sum_x \vec{s}_x . \quad (2)$$

The geometry of the lattice is the same as above for the Blume-Capel model. Whereas the field takes the values

$$\vec{s}_x \in \{(0, 0), (\cos(2\pi m/q), \sin(2\pi m/q))\} , \quad (3)$$

where $m \in \{1, \dots, q\}$. Compared with the q -state clock model, $(0, 0)$ is added as possible value of the field variable. Here we perform simulations for a vanishing external field $\vec{H} = \vec{0}$. Note that, following the convention of, for example [13, 25], the parameter D has the opposite sign as for the Blume-Capel model, Eq. (1). In the simulation program we use a label $m \in \{0, \dots, q\}$ to store the spins:

$$\vec{s}(0) = (0, 0) \quad (4)$$

and for $m > 0$

$$\vec{s}(m) = (\cos(2\pi m/q), \sin(2\pi m/q)) . \quad (5)$$

We introduce the weight factor

$$w(\vec{s}_x) = \delta_{0,\vec{s}_x} + \frac{1}{q} \delta_{1,\vec{s}_x} = \delta_{0,m_x} + \frac{1}{q} \sum_{n=1}^q \delta_{n,m_x} \quad (6)$$

that gives equal weight to $(0,0)$ and the collection of all values $|\vec{s}_x| = 1$. Now the partition function can be written as

$$Z = \sum_{\{\vec{s}\}} \prod_x w(\vec{s}_x) \exp(-\mathcal{H}_{q+1}), \quad (7)$$

where $\{\vec{s}\}$ denotes a configuration of the field. The weight, Eq. (6), is introduced to get the measure of the dynamically diluted XY (ddXY) model [21, 25]

$$d\mu(\vec{s}_x) = ds_x^{(1)} ds_x^{(2)} \left[\delta(\phi_x^{(1)}) \delta(\phi_x^{(2)}) + \frac{1}{2\pi} \delta(1 - |\vec{\phi}_x|) \right] \quad (8)$$

in limit $q \rightarrow \infty$.

For reasons that become clear below, we do not simulate at general (D, K_3) , but only the two limiting cases $K_3 = 0$ or $D \rightarrow \infty$. For $K_3 = 0$ we get the model studied in Ref. [13]. Here we perform new simulations for $q = 12$ at criticality. Our main focus is however on simulations for $D \rightarrow \infty$, where the relative weight of $\vec{s}_x = (0,0)$ vanishes. Hence we simulate the q -state clock model with nearest and next-to-next-to-nearest neighbor interactions defined by the reduced Hamiltonian

$$\mathcal{H}_q = -K_1 \sum_{\langle xy \rangle} \vec{s}_x \cdot \vec{s}_y - K_3 \sum_{[xy]} \vec{s}_x \cdot \vec{s}_y - \vec{H} \cdot \sum_x \vec{s}_x, \quad (9)$$

where the field takes the values

$$\vec{s}_x \in \{(\cos(2\pi m/q), \sin(2\pi m/q))\}, \quad (10)$$

where $m \in \{1, \dots, q\}$. All q possible values of the spin have the same weight. Below, we denote this model by 3N q -state clock model.

A. Definitions of the measured quantities

The quantities studied in FSS are the same as in [13]. For completeness we list them below: The energy density is defined as

$$E = \frac{1}{V} \sum_{\langle xy \rangle} \vec{s}_x \cdot \vec{s}_y. \quad (11)$$

The magnetic susceptibility χ for a vanishing magnetization and the second moment correlation length ξ_{2nd} are defined as

$$\chi = \frac{1}{V} \left\langle \left(\sum_x \vec{s}_x \right)^2 \right\rangle \quad (12)$$

and

$$\xi_{2nd} = \sqrt{\frac{\chi/F - 1}{4 \sin^2 \pi/L}}, \quad (13)$$

where

$$F = \frac{1}{V} \left\langle \left| \sum_x \exp \left(i \frac{2\pi x_1}{L} \right) \vec{s}_x \right|^2 \right\rangle \quad (14)$$

is the Fourier transform of the correlation function at the lowest non-zero momentum. We consider several dimensionless quantities, which are also called phenomenological couplings. These quantities are invariant under renormalization group (RG) transformations. We consider the Binder cumulant U_4 and its sixth-order generalization U_6 , defined as

$$U_{2j} = \frac{\langle (\vec{m}^2)^j \rangle}{\langle \vec{m}^2 \rangle^j}, \quad (15)$$

where $\vec{m} = \frac{1}{V} \sum_x \vec{s}_x$ is the magnetization of the system. We also consider the ratio $R_Z = Z_a/Z_p$ of the partition function Z_a of a system with anti-periodic boundary conditions in one of the three directions and the partition function Z_p of a system with periodic boundary conditions in all directions. Anti-periodic boundary conditions in 0-direction are obtained by changing the sign of the term $\vec{s}_x \cdot \vec{s}_y$ of the Hamiltonian for links $\langle xy \rangle$ that connect the boundaries, i.e., for $x = (L-1, x_1, x_2)$ and $y = (0, x_1, x_2)$. In order to avoid microscopic effects at the boundary, we require that $-\vec{s}_x$ is in the same set of values as \vec{s}_x . Hence we take even values of j . In the following we refer to dimensionless ratios by R . Derivatives of dimensionless ratios with respect to the inverse temperature

$$S_R = \frac{\partial R}{\partial K_1} \quad (16)$$

are used to determine the critical exponent ν . In the following these quantities are also denoted by slope of R . Note that here we decided ad hoc to take the partial derivative with respect to K_1 at fixed K_3 and D . Taking the derivative with respect to a linear combination of K_1 and K_3 would also be a viable choice. For example, in Ref. [8], we pass the critical line at a fixed ratio of K_3/K_1 . We did not implement both the derivatives with respect to K_1 and K_3 , to avoid the handling of additional data.

In the FSS analysis we need the observables as a function of K_1 in a certain neighborhood of the critical coupling $K_{1,c}$. To this end, we simulate at $K_{1,s}$, which is a good approximation of $K_{1,c}$. In order to extrapolate in K_1 we compute the coefficients of the Taylor series in $K_1 - K_{1,s}$ for all quantities listed above up to the third order. Note that a reweighting analysis is not possible, since, due to the large statistics, we performed a binning of the data already during the simulation.

III. CORRECTIONS TO SCALING

In the analysis of our data, corrections to scaling have to be taken into account. These corrections are either caused by irrelevant scaling fields or are intrinsic to the observables. These intrinsic corrections can be related in some cases to redundant scaling fields of certain RG transformations. An example of such a correction is the analytic background in the magnetic susceptibility. The operators associated with the scaling fields can be classified according to the spatial symmetry, the internal symmetry and their dimension. For a nice discussion see Sec. 3 of Ref. [26].

First we discuss the corrections related to finite values of q . These are well understood and the corresponding RG exponent Y_q is rapidly decreasing with increasing q . We shall use values of q such that these corrections can be safely ignored in the analysis of our data. Note that we stay in the neighborhood of the critical point. Hence the dangerously irrelevant character [27, 28] of the perturbation can be ignored.

Next we summarize results for the leading correction exponent ω and the subleading correction exponent ω_{NR} . Note that the subleading correction is due to the breaking of the spatial rotational invariance by the lattice.

A. Dependence of the physics on q

Let us summarize results on the RG eigenvalues Y_q of a \mathbb{Z}_q -invariant perturbation at the $O(2)$ -invariant fixed point. For large values of q one gets

$$\Delta_q = c_{3/2}q^{3/2} + c_{1/2}q^{1/2} + c_0 + O(q^{-1/2}), \quad (17)$$

where $Y_q = 3 - \Delta_q$. See Ref. [29] and references therein. This has been checked numerically in Refs. [30, 31]. In Ref. [31] the estimates $c_{3/2} = 0.340(1)$ and $c_{1/2} = 0.23(2)$ are provided,

consistent with Ref. [30]. The value $c_0 \simeq -0.0937$ is predicted theoretically. Plugging in these numbers in Eq. (17) we get for example $Y_q = 2.52, 1.81, 0.93, -0.09, -1.22, \dots, -5.25, \dots, -11.83, \dots, -19.59$ for $q = 1, 2, 3, 4, 5, \dots, 8, \dots, 12, \dots, 16$. Comparing with, for example, $Y_2 = 1.7639(11)$, $Y_3 = 0.8915(20)$, $Y_4 = -0.108(6)$, Ref. [32], or $Y_2 = 1.76371(11)$, Ref. [14], we see that Eq. (17) is reasonably accurate down to small values of q . Even in the case $Y_1 = y_h = 2.480912(22)$, Ref. [14], the estimate obtained from Eq. (17) is close. For our purpose, it is important to note that Y_q is negative for $q \geq 4$ and rapidly decreases with increasing q . For example, for $q = 8$, which we considered in Ref. [13], $Y_8 \approx -5.25$. In the present work, the smallest value of q we simulated at is $q = 12$.

Next let us discuss whether the $(q + 1)$ -state clock model, for $q \geq 4$, at criticality, is in the basin of attraction of the $O(2)$ -invariant fixed point. It is easy to see that the 4-state clock model is equivalent to two decoupled Ising systems by writing the two components of the field as $s^{(1)} = \frac{1}{2}(\sigma + \tau)$ and $s^{(2)} = \frac{1}{2}(\sigma - \tau)$, where $\sigma, \tau \in \{-1, 1\}$, see for example Ref. [33]. Hence the 4-state clock model is not in the basin of attraction of the $O(2)$ -invariant fixed point. For a finite value of D we have no definite answer. For $q = 5$ it is demonstrated numerically in Ref. [33] that the model undergoes a second order phase transition, where the $O(2)$ symmetry is restored. This is confirmed for example in Ref. [34]. It is plausible that the same holds for $q > 5$. For $q = 6$ this has been confirmed numerically, for example, in Ref. [34]. For certain finite values of D this has been demonstrated for $q = 6, 7, 8$, and 10 in Ref. [13].

Note that the \mathbb{Z}_q -invariant perturbation for $q \geq 4$ is dangerously irrelevant [27, 28]. In the low temperature phase, in the thermodynamic limit, the magnetization might only point in one of the q directions given by Eq. (5). However this does not affect the FSS study in the neighborhood of the critical point that is performed here.

For $q \geq 5$ and finite D there is a range $[\infty, D_{tri})$, where the transition is continuous. For $D < D_{tri}$ it becomes first order. In Ref. [13] we find $-0.87 < D_{tri} < -0.86$ for $q = 8$ and $K_3 = 0$. For larger q the value of D_{tri} should virtually not change. The values of D simulated below are clearly in the second order range.

In ref. [13] we find, that at the level of our numerical accuracy, the estimate of $K_{1,c}$ becomes indistinguishable from the $q \rightarrow \infty$ limit for $q \gtrsim 10$. In the present study we simulate $q \geq 12$. Hence we expect that even for non-universal quantities, the numerical estimates obtained here are, within the quoted errors, valid for the $q \rightarrow \infty$ limit.

B. Correction exponents for the XY universality class

In the case of the three-dimensional Ising universality class accurate results for the dimensions of various operators obtained by using CB are provided in Ref. [10]. These results are corroborated by fuzzy sphere calculations [35]. For a summary of results obtained by using the ϵ -expansion and the $1/N$ -expansion for general N see Ref. [26]. These results show that, at least for the leading corrections, the spectrum of correction exponents is sparse. This is actually the reason why we can improve models by tuning a single parameter. Or as discussed here by tuning two parameters. Field theory suggests that this qualitative property also holds for $N > 1$, where N refers to the $O(N)$ symmetry of the theory [26].

Let us turn to the XY universality class. The leading correction exponent $\omega = \Delta_{s'} - 3$ is known from field theory, functional renormalization group, Monte Carlo simulations, and the CB. In [13] we find $\omega = 0.789(4)$, which is fully consistent with the CB estimate $\Delta_{s'} = 3.794(8)$ given in table 4 of Ref. [14]. In Ref. [36] the authors find $\omega = 0.791(8)$ by using the functional renormalization group (FRG). The subleading correction is due to the violation of spatial rotational invariance by the simple cubic lattice. Here we are aiming at the leading correction, which is associated with spin $l = 4$. From Fig. 3 of Ref. [37, 38] $\omega_{NR} = 2.02548(41)$. Note that the value of ω_{NR} is only slightly larger than that for the Ising universality class. Analyzing the ϵ -expansion and the $1/N$ -expansion of ω_{NR} [39, 40], where the coefficients are taken from Ref. [26], we conclude that for the Heisenberg universality class ω_{NR} takes a similar value as for the XY universality class, and then monotonically decreases with increasing N , reaching $\omega_{NR} = 2$ in the limit $N \rightarrow \infty$. Note that $\omega_{NR} = 2$ is the result for a free field theory. Note that in the case of the Ising universality the subleading correction exponent for $l = 4$ is $\omega'_{NR} = 3.42065(64)$ given in table 2 of [10]. In Fig. 3 of Ref. [37] we see that ω_l rapidly increases with l . For example for $l = 8$ one gets $\omega_{l=8} \approx 6.03$.

C. Dependence of the amplitudes of corrections on the parameters

Finite size scaling (FSS) determines the behavior of dimensionless quantities at the critical point on a finite lattice. As example let us consider the ratio of partition functions at criticality

$$[Z_a/Z_p](L, D, K_{1,c}, r_K) = [Z_a/Z_p]^* + b(D, r_K)L^{-\omega} + d b^2(D, r_K)L^{-2\omega} + \dots$$

$$+c(D, r_K)L^{-\omega_{NR}} + \dots, \quad (18)$$

where $r_K = K_3/K_1$. Here we assume a lattice with the linear lattice size $L = L_0 = L_1 = L_2$ with periodic boundary conditions. Note that RG predicts that the amplitudes of the corrections in other quantities are proportional to the ones of Z_a/Z_p , since they originate from the same scaling fields. Finding an improved model means finding (D, r_K) such that $b(D, r_K) = 0$. To this end, varying a single parameter is actually sufficient. Note that a priori it is not guaranteed that such a zero exists for the model studied. Here we attempt to find a point in the parameter space, where both amplitudes $b(D, r_K)$ and $c(D, r_K)$ vanish. In order to develop a strategy to find these zeros, a qualitative understanding of the dependence of $b(D, r_K)$ and $c(D, r_K)$ on their arguments is helpful. It is plausible that the behavior is qualitatively the same as in the case of the Blume-Capel model with next and third next nearest neighbor interactions that we studied in Ref. [8]. The first proposition is that $c(D, r_K)$, for fixed r_K , depends very little on D , while $b(D, r_K)$ strongly depends on D . On the other hand, for fixed D , both $b(D, r_K)$ and $c(D, r_K)$ have a clear dependence on r_K . Based on the results for the Blume-Capel model, we expect that, at least for small $r_K > 0$, increasing r_K has qualitatively the same effect on $b(D, r_K)$ as decreasing D . Hence a point in the (D, r_K) plane with $b(D, r_K) = 0$ and $c(D, r_K) = 0$ can only be found if $r_K^* \geq r_K^{iso}$ for $D \rightarrow \infty$, where r_K^* is the zero of b and r_K^{iso} the zero of c . In Fig. 1 we sketch the behavior of the zeros of the correction amplitudes discussed above.

IV. RESTORING ISOTROPY

In a typical FSS setting with $\xi_{\text{exp}} \gtrsim L$, where ξ_{exp} is the exponential correlation length in the thermodynamic limit, it is difficult to detect the violation of the rotational invariance that is caused by the lattice. This is due to the fact that rotational invariance is also broken by the torus geometry of the system with periodic boundary conditions. To avoid this problem, we simulate in the high temperature phase such that $\xi_{\text{exp}} \ll L$. Here, the correlation function at distances considerably smaller than the lattice size is barely affected by the torus geometry.

The simulations in the high temperature phase were performed by using the single cluster algorithm [7]. In the case of the $(q + 1)$ -state clock model with finite D , local updates that allow the transition from $s_x = 0$ to $|s_x| = 1$ and vice versa were used in addition. For a

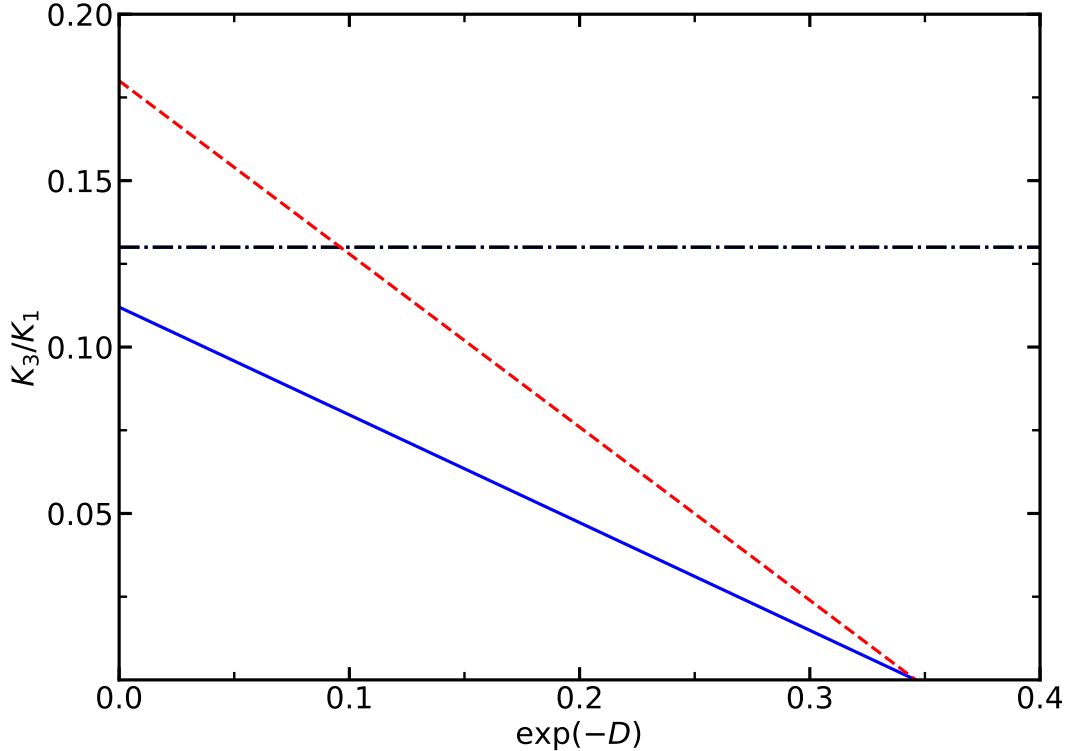


FIG. 1. We sketch possible scenarios for the zeros of the leading correction amplitude $b(D, r_K)$ and the subleading correction amplitude $c(D, r_K)$. The straight dash-dotted line gives $c(D, r_K) = 0$, while the straight solid line and the dashed line give two a priori possible behaviors of $b(D, r_K) = 0$. The plot resembles the qualitative behavior discussed in the text: Since $c(D, r_K)$ depends weakly on D , the zero occurs at an approximately constant value of r_K . Here we have used the value of r_K^{iso} for $D \rightarrow \infty$ that we shall find below in Sec. IV. In the case of $b(D, r_K) = 0$ we have used $D^* \approx 1.06$ for $K_3 = 0$ from Ref. [13] as one endpoint. For $D \rightarrow \infty$ we find below $r_K^* < r_K^{iso}$ and there is no intersection of the zeros of $b(D, r_K)$ (solid line) and $c(D, r_K) = 0$. The dashed line gives qualitatively the result obtained for the Blume-Capel model with 3N couplings. Here we get an intersection at a finite value of D .

more detailed discussion of such a hybrid update scheme see for example Sec. IV of Ref. [13]. The numerical study presented below is similar to the one discussed in Sec. IV of Ref. [8] for the Ising universality class in three dimensions.

Below, we first simulate $K_3 = 0$ at $D \approx D^*$ and $D \rightarrow \infty$ to establish so to speak the baseline and to check that the behavior of the spatial unisotropy is compatible with the theoretical prediction for the exponent ω_{NR} . Then, for $D \rightarrow \infty$, we search for r_K^{iso} , where

the leading contribution to the spatial unisotropy vanishes.

A. The correlation length in the high temperature phase

In order to quantify spatial anisotropy, we determine the correlation length in three different directions of the lattice. Below we discuss how the correlation length is determined. We start with the definition of the basic quantities.

Slice averages are given by

$$\vec{S}_{(1,0,0)}(x_0) = \sum_{x_1, x_2} \vec{s}_{x_0, x_1, x_2} , \quad (19)$$

where the slice is perpendicular to the $(1, 0, 0)$ -axis. In addition, we consider slices perpendicular to the $(1, 1, 0)$ and the $(1, 1, 1)$ -axis. The corresponding slice averages are given by

$$\vec{S}_{(1,1,0)}(x_0) = \sum_{x_1, x_2} \vec{s}_{x_0 - x_1, x_1, x_2} \quad (20)$$

and

$$\vec{S}_{(1,1,1)}(x_0) = \sum_{x_1, x_2} \vec{s}_{x_0 - x_1 - x_2, x_1, x_2} . \quad (21)$$

Note that the arithmetics of the coordinates is understood modulo the linear lattice size L . The distance between adjacent slices is $d_s = 1, 2^{-1/2}$, and $3^{-1/2}$ for slices perpendicular to the $(1, 0, 0)$ -, $(1, 1, 0)$ - and the $(1, 1, 1)$ -axis, respectively. Going from a site in the direction of the $(1, 1, 0)$ - and the $(1, 1, 1)$ -axis, we hit the next site in the second and the third next slice, respectively. The slice correlation function is defined as

$$G_r(t) = \langle \vec{S}_r(x_0) \cdot \vec{S}_r(x_0 + t) \rangle , \quad (22)$$

where $r = (1, 0, 0), (1, 1, 0)$, or $(1, 1, 1)$ and $x_0 + t$ is understood modulo the linear lattice size L .

In our simulations, in order to reduce the statistical error, we average over all x_0 and all directions equivalent to those given by the $(1, 0, 0)$ -, $(1, 1, 0)$ - and the $(1, 1, 1)$ -axis, respectively. The correlation function is determined by using the variance reduced estimator associated with the cluster algorithm [6, 7]. We define the effective correlation length in direction r by

$$\xi_{r,eff}(t) = \frac{sd_r}{\ln(G_r(t)/G_r(t+s))} , \quad (23)$$

where $L \gg t$ is assumed, d_r is the distance between adjacent slices and s is a stride. Here we take $s = 1, 2$, and 3 for $r = (1, 0, 0)$, $(1, 1, 0)$, and $(1, 1, 1)$, respectively. To relax $L \gg t$ to some extent, we take the periodicity of the lattice into account. To this end we solve numerically

$$G_r(t) = c \left(\exp \left(-\frac{d_r t}{\xi_{r,eff}(t)} \right) + \exp \left(-\frac{d_r(L-t)}{\xi_{r,eff}(t)} \right) \right), \quad (24)$$

$$G_r(t+s) = c \left(\exp \left(-\frac{d_r(t+s)}{\xi_{r,eff}(t)} \right) + \exp \left(-\frac{d_r(L-t-s)}{\xi_{r,eff}(t)} \right) \right). \quad (25)$$

Similar to the Ising universality class in three dimensions, in the high temperature phase $\xi_{r,eff}(t)$ converges quickly as $t \rightarrow \infty$. See Ref. [41, 42] and references therein.

In a set of preliminary simulations, we determined the lattice size L and distance t that is needed to keep deviations from the desired limit $L \rightarrow \infty$ followed by $t \rightarrow \infty$ at a size smaller than the statistical error. We conclude that $d_r t \simeq 2\xi_r$ and $L \simeq 20\xi_r$ is sufficient. In the following we take $\xi_{r,eff}(t)$ at $d_r t \simeq 2\xi_r$ as estimate of the correlation length ξ_r . In order to quantify the spatial anisotropy, we study the ratios

$$r_2 = \frac{\xi_{(1,0,0)}}{\xi_{(1,1,0)}}, \quad r_3 = \frac{\xi_{(1,0,0)}}{\xi_{(1,1,1)}} \quad (26)$$

in the neighborhood of the critical point. Note that for the ratios r_2 and r_3 , the covariance between the correlation lengths in the different directions are properly taken into account by performing a Jackknife analysis.

We expect

$$r_i - 1 = a_i(D, r_K) \xi_{(1,0,0)}^{-\omega_{NR}} + b_i(D, r_K) \xi_{(1,0,0)}^{-\omega'_{NR}} + \dots \quad (27)$$

B. Numerical results for the $(q+1)$ -state clock model at $K_3 = 0$

First we determine the correlation length in three directions for the $(q+1)$ -state clock model at $K_3 = 0$. In our simulations we take $q = 16$. We simulated at $D = 1.05$ and 1.07 , which are close to D^* . In Ref. [13] we find $D^* = 1.058(13)$ for $q = 8$. For larger values of q , D^* should change only by little. In particular $|D^*(q=10) - D^*(q=8)| \leq 0.0005$ is estimated in Ref. [13]. Our numerical results for the correlation length are summarized in table I. For example for $D \rightarrow \infty$, $K_1 = 0.44049$ we performed about 2×10^{11} single cluster updates.

TABLE I. We give estimates of the correlation length $\xi_{(1,0,0)}$ and the ratios r_2 and r_3 for the $(16+1)$ -state clock model with nearest neighbor couplings only at $D = 1.05, 1.07$ and ∞ . L is the linear lattice size and K_1 the nearest neighbor coupling. For a discussion see the text.

| D | K_1 | L | $\xi_{(1,0,0)}$ | r_2 | r_3 | $(r_2 - 1)\xi_{(1,0,0)}^{2.02548}$ | $(r_3 - 1)\xi_{(1,0,0)}^{2.02548}$ |
|----------|----------|-----|-----------------|-------------|-------------|------------------------------------|------------------------------------|
| 1.05 | 0.53185 | 60 | 3.01417(5) | 1.002258(6) | 1.003022(7) | 0.02110(6) | 0.02824(7) |
| 1.05 | 0.54186 | 80 | 4.02463(7) | 1.001263(6) | 1.001698(8) | 0.02120(10) | 0.02850(12) |
| 1.05 | 0.547185 | 100 | 5.03384(9) | 1.000800(5) | 1.001076(6) | 0.02112(13) | 0.02841(16) |
| 1.05 | 0.55042 | 120 | 6.04634(7) | 1.000562(3) | 1.000759(4) | 0.02151(12) | 0.02905(15) |
| 1.07 | 0.5398 | 80 | 4.00873(5) | 1.001272(5) | 1.001705(6) | 0.02118(8) | 0.02839(10) |
| ∞ | 0.4258 | 60 | 3.01208(4) | 1.002254(5) | 1.003016(6) | 0.02103(5) | 0.02814(6) |
| ∞ | 0.4353 | 80 | 4.00646(5) | 1.001276(6) | 1.001713(7) | 0.02122(10) | 0.02849(12) |
| ∞ | 0.44049 | 100 | 5.00670(5) | 1.000810(5) | 1.001090(6) | 0.02115(13) | 0.02847(16) |

As expected, for $D = 1.05$, we see that $(r_i - 1)\xi_{(1,0,0)}^{2.02548}$ stays roughly constant with increasing correlation length. The estimates of r_i for $\xi_{(1,0,0)} \approx 4$ for $D = 1.05$ and 1.07 are consistent. The estimates of $(r_i - 1)\xi_{(1,0,0)}^{2.02548}$ for $D \rightarrow \infty$ and $D = 1.05$ are equal within the statistical error. This confirms the hypothesis that the violation of isotropy depends little on D .

C. Numerical results for the q -state clock model at $K_3 > 0$

Next we studied the 3N q -state clock model. As above, we take $q = 16$. Here we aim at finding $r_K^{iso} = K_3/K_1$, where rotational invariance is restored.

Based on preliminary simulations, we have chosen K_1 and K_3 such that $\xi_{(1,0,0)} \approx 3, 4, 5$, or 6 . Furthermore r_K is chosen such that the deviation of r_2 and r_3 from one is small. Our numerical results are summarized in table II. Throughout the linear lattice size is chosen such that $L \approx 20\xi_{(1,0,0)}$ except for $(K_1, K_3) = (0.3372, 0.044)$, where we have simulated $L = 80$ in addition to $L = 60$ to check that finite size effects are not larger than the statistical error.

In the first step of the analysis, we determine the zeros of $r_2 - 1$ and $r_3 - 1$ for each

value of $\xi_{(1,0,0)}$. To this end, we performed a linear fit of $r_i - 1$ in r_K . In the case of $r_2 - 1$, we get $r_K^{iso} = 0.12744(29)$, $0.12919(36)$, $0.12832(60)$, and $0.12926(87)$ for $\xi_{(1,0,0)} \approx 3, 4, 5$, and 6 , respectively. The corresponding numbers for $r_3 - 1$ are $0.12729(25)$, $0.12950(32)$, $0.12953(52)$, and $0.13107(74)$. We note that the estimates obtained from r_2 and r_3 are consistent. We expect that corrections decay as $\xi_{(1,0,0)}^{-\omega'_{NR} + \omega_{NR}}$. For the critical limit, we arrive at

$$r_K^{iso} = 0.132(2) , \quad (28)$$

where the error is chosen such that it covers both the estimates obtained from r_2 and r_3 . Note that for the free field theory one gets $r_K^{iso} = 0.125$ [43] and $r_K^{iso} = 0.129(1)$ for the Blume-Capel model with nearest neighbor and next-to-next-to-nearest neighbor interactions [8].

V. SIMULATIONS AT CRITICALITY

In this section we discuss the simulations performed close to the critical point, such that $\xi \gg L$. We analyze data for $q = 8$, $K_3 = 0$ at $D = 1.02, 1.05$, and 1.07 . These were already generated for Ref. [13]. For $q = 12$, $K_3 = 0$ we generated new data at $D = 1.05, 1.06$, and 1.07 . Our main focus is on $D \rightarrow \infty$, $K_3 > 0$. Here $q \geq 24$ throughout. We simulated at $K_3 = 0.04, 0.0415, 0.042, 0.046$, and 0.05 . These values of D and K_3 are close to D^* and K_3^* , respectively. In the following, we briefly discuss the algorithm that has been used for the simulations. Then we summarize the lattice sizes that have been simulated and the statistics that we achieved in our simulations.

First we analyze the dimensionless quantities Z_a/Z_p , ξ_{2nd}/L , U_4 and U_6 , defined in Sec. II A. We obtain estimates of the fixed point values of these dimensionless quantities and estimates of the zeros of the leading correction amplitude D^* and K_3^* . We confirm the estimate of r_K^{iso} obtained in the previous section. We get accurate estimates of $K_{1,c}(D, K_3)$.

Then we compute the critical exponent η by analyzing the magnetic susceptibility χ at criticality and the RG exponent $y_t = 1/\nu$ by analyzing slopes $S_R = \frac{\partial R}{\partial K}$ of dimensionless quantities at criticality.

TABLE II. Estimates of the correlation length $\xi_{(1,0,0)}$ and the ratios r_2 and r_3 for the 16-state clock model with next and next-to-next-to-nearest neighbor coupling constants. L is the linear lattice size and K_1 and K_3 are the coupling constants. For a discussion see the text.

| K_1 | K_3 | K_3/K_1 | L | $\xi_{(1,0,0)}$ | r_2 | r_3 |
|---------|---------|--------------|-----|-----------------|-------------|-------------|
| 0.347 | 0.039 | 0.1123919... | 60 | 3.02338(3) | 1.000187(5) | 1.000247(5) |
| 0.3448 | 0.04 | 0.1160092... | 60 | 3.00471(3) | 1.000140(5) | 1.000186(6) |
| 0.341 | 0.042 | 0.1231671... | 60 | 3.01011(3) | 1.000054(5) | 1.000067(6) |
| 0.3372 | 0.044 | 0.1304863... | 60 | 3.01430(3) | 0.999962(5) | 0.999948(6) |
| 0.3372 | 0.044 | 0.1304863... | 80 | 3.01431(2) | 0.999962(4) | 0.999944(5) |
| 0.3548 | 0.04 | 0.1127395... | 80 | 4.02702(3) | 1.000100(5) | 1.000145(6) |
| 0.347 | 0.044 | 0.1268011... | 80 | 4.01415(3) | 1.000013(4) | 1.000021(5) |
| 0.34556 | 0.0447 | 0.1293552... | 80 | 4.00013(3) | 1.000001(4) | 1.000003(5) |
| 0.34316 | 0.046 | 0.1340482... | 80 | 4.01300(3) | 0.999970(4) | 0.999961(5) |
| 0.36 | 0.04 | 0.1111111... | 100 | 5.02203(4) | 1.000080(4) | 1.000112(5) |
| 0.3582 | 0.041 | 0.1144611... | 100 | 5.05559(4) | 1.000062(4) | 1.000088(5) |
| 0.3523 | 0.044 | 0.1248935... | 100 | 5.02358(4) | 1.000013(4) | 1.000026(5) |
| 0.3484 | 0.046 | 0.1320321... | 100 | 5.00579(3) | 0.999985(4) | 0.999986(4) |
| 0.3516 | 0.046 | 0.1308304... | 120 | 5.99989(3) | 0.999995(3) | 1.000001(3) |
| 0.3621 | 0.04054 | 0.1119580... | 120 | 6.00411(4) | 1.000055(4) | 1.000079(4) |

A. The simulation program/algorithm

We simulated the model by using a hybrid of the Metropolis, the single cluster [7] and the wall cluster algorithm [44]. For finite D , the Metropolis updates are needed to update $\vec{s}_x = (0, 0)$ to $|\vec{s}_x| = 1$ and vice versa. For a discussion see Sec. IV of Ref. [13]. In the case of $K_3 > 0$ and $D \rightarrow \infty$, we kept the Metropolis updates, even though they are not required. During the study the precise composition of the update cycle changed. The advantage of simulating with finite q is that delete probabilities for the cluster algorithm and acceptance probabilities for the Metropolis algorithm can be computed at the beginning of the simulation and be stored in a lookup table. Furthermore, for the values of q considered

here, 8 bit `char` variables are sufficient to store the spins. Note that the efficiency of the hybrid update does not depend sharply on the precise composition of the update cycle. In our most recent simulations for $K_3 > 0$ and $D \rightarrow \infty$ we have used

```
for(i=0;i<N_bin;i++)
{
for(k=0;k<3;k++)
{
metropolis();
for(l=0;l <L/4;l++) single_cluster();
2 times wall_cluster(direction=k);
measurements();
}
}
```

In the pseudo-C code given above, `metropolis()` is a sweep with the local Metropolis over the lattice. `single_cluster()` is one single cluster update. The average size of a single cluster, at the critical point, grows like $L^{2-\eta}$. Hence performing $L/4$ single cluster updates in one update cycle, the fraction of updated sites stays roughly constant with increasing linear lattice size L . `wall_cluster(direction=k)` is the wall cluster update. It is performed for planes perpendicular to the $(1, 0, 0)$, $(0, 1, 0)$, and $(0, 0, 1)$ -axis in a sequence. In order to compute Z_a/Z_p we need two subsequent wall cluster updates, where the two reflection axes are perpendicular. In Ref. [25] the authors find that for the ddXY model the average size W of the wall cluster behaves as $W = aL^{2.512}$, where the error of the exponent is not given. Here, for $K_3 = 0.0415$ and $K_1 \approx K_{1,c}$ we get $W = aL^{2.4828(3)} + bL^{1.863(6)}$ with acceptable fits starting from $L \approx 20$. We made no effort to estimate systematic errors in the values of the exponents. This result means that the fraction of time spent with the wall cluster update decreases with increasing lattice size.

In the major part of the simulations we have used a hybrid of generators, where one component is the `xoshiro256+` taken from [45]. For a discussion of the generator see [46]. As second component we used a 96 bit linear congruential generator with the multiplier and the increment $a = c = 0xc580cadd754f7336d2eaa27d$ and the modulus $m = 2^{96}$ suggested by O'Neill [47]. In this case we used our own implementation. The third component is

a multiply-with-carry generator taken from [48]. For a more detailed discussion see the Appendix A of Ref. [8].

In preliminary runs with about 10^6 update cycles at our preliminary estimate of $K_{1,c}$ for $K_3 = 0.0415$ we determined the integrated autocorrelation times of the energy density and the magnetic susceptibility. For the update cycle given above, in units of measurements, we find for example that $\tau_{int,ene} = 3.45(3)$ and $6.16(8)$ for $L = 40$ and 200 , respectively. The integrated autocorrelation time of the magnetic susceptibility is smaller: $\tau_{int,\chi} = 2.94(3)$ and $3.73(5)$ for $L = 40$ and 200 , respectively. The autocorrelation times grow slowly with increasing lattice size. Since the fraction of sites that are updated by the wall cluster shrinks with increasing linear lattice size, we abstain from quoting an estimate of the dynamical critical exponent z .

B. The data

For $D \rightarrow \infty$, we have generated data for $K_3 = 0.04, 0.0415, 0.042, 0.046, \text{ and } 0.05$. The simulations were performed at iteratively improved estimates of $K_{1,c}(K_3)$. The highest statistics is achieved for $K_3 = 0.0415$, which is close to our final estimate of K_3^* . Here we simulated the linear lattice sizes $L = 8, 9, \dots, 20, 22, \dots, 36, 40, \dots, 72, 80, 90, 100, 120, 140, 160, \text{ and } 200$. For example for $L = 24, 64, 100, 140, \text{ and } 200$, we performed about 1.4×10^{10} , 3.3×10^9 , 8.9×10^8 , 6.4×10^8 , and 3×10^8 measurements. The statistics is monotonically decreasing with increasing lattice size, while the CPU time that is used is increasing with the lattice size. In total we used roughly the equivalent of 60 years on a single core of an Intel(R) Xeon(R) CPU E3-1225 v3 running at 3.20 GHz for the simulations at $K_3 = 0.0415$.

By mistake, for some of the runs at $K_3 = 0.042$ and 0.046 we did not compute ξ_{2nd}/L correctly. This actually triggered us to perform a joint analysis of Z_a/Z_p and U_4 only, instead of $Z_a/Z_p, \xi_{2nd}/L, U_4$ and U_6 in the section below.

For $q = 12$ and $K_3 = 0$, we simulated at $D = 1.05, 1.06, \text{ and } 1.07$. First simulations, already performed a few years back, were performed by using the SIMD-oriented Fast Mersenne Twister (SMFT) [49] pseudo-random number generator, where SIMD is the abbreviation for single instruction, multiple data. For $D = 1.05$ and 1.07 we performed simulations for the linear lattice sizes $L = 5, 6, \dots, 14, 16, \dots, 24, 28, \dots, 40, 48, \dots, 72$. For $D = 1.06$ we simulated in addition $L = 15, 26, 30, 44, 80, \text{ and } 100$. For $D = 1.06$, up to

$L = 28$, we performed about 7×10^9 measurements. The number of measurement is then decreasing to 6×10^8 for $L = 100$. In total the equivalent of about 20 years on a single core of an Intel(R) Xeon(R) CPU E3-1225 v3 running at 3.20 GHz are used for these simulations.

C. Finite size scaling of dimensionless quantities

We analyze dimensionless quantities for $q = 8$ at $D = 1.02, 1.05$ and 1.07 , and $q = 12$ at $D = 1.05, 1.06$ and 1.07 , where in all cases $K_3 = 0$, and $K_3 = 0.04, 0.0415, 0.042, 0.046$, and 0.05 for $D \rightarrow \infty$. The data for $q = 8, K_3 = 0$ were generated for Ref. [13]. For a discussion of the theoretical background of the FSS analysis performed here see Refs. [13, 21, 25]. First we jointly fit the ratio of partition functions Z_a/Z_p and the Binder cumulant U_4 . We use Ansätze of the form

$$R_i(L, D, K_1, K_3)|_{K_1=K_{1,c}} = R_i^* + \sum_{j=1}^{j_{max}} c_{i,j}(D, K_3)L^{-\epsilon_j} . \quad (29)$$

Note that we have simulated at $K_{1,s} \approx K_{1,c}$. In addition to the value of $R_i(L, D, K_{1,s}, K_3)$, we determine the Taylor coefficients of the expansion of R_i in $(K_1 - K_{1,s})$ up to the third order. In our fits, we keep $R_i(L, D, K_{1,s}, K_3)$ on the right side of the equation, and bring the terms proportional to $(K_1 - K_{1,s})^\alpha$ for $\alpha = 1, 2$, and 3 to the left. Furthermore, we ignore the statistical error of the Taylor coefficients. This way, we can treat $K_{1,c}$ as a free parameter in the fit.

We perform fits with $j_{max} = 3$, where we take the correction exponents $\epsilon_1 = \omega$, $\epsilon_2 = 2 - \eta$, and $\epsilon_3 = \omega_{NR}$, with the numerical values $\omega = 0.789$, $\eta = 0.03817$, and $\omega_{NR} = 2.02548$. For a discussion see Sec. III B. As check we performed fits with $j_{max} = 4$, taking $\epsilon_4 = 3.6$. We ignore corrections proportional to $L^{-2\omega}$ or $L^{-\omega-\omega_{NR}}$, since for the values of D and K_3 that we simulate at, $|b_i(D, K_3)|$ is small.

Let us discuss the parameterization of $c_{i,j}(D, K_3)$. First we note that Z_a/Z_p is not affected by the analytic background of the magnetization. Hence $c_{Z_a/Z_p,2} = 0$. Furthermore, RG predicts that $c_{i,j}(D, K_3) = r_{ilj}c_{l,j}(D, K_3)$, since they originate from the same scaling field.

RG predicts that the amplitudes $c_{i,j}(D, K_3)$ are smooth functions. Here we consider values of D and K_3 in a small range around D^* and K_3^* , respectively. Therefore we approximate $c_{i,j}(D, K_3)$ by low order Taylor approximations, for the two cases $K_3 = 0$ and $D \rightarrow \infty$. Our first parameterization for $j_{max} = 3$ is

for $K_3 = 0$:

$$\begin{aligned}
c_{U_4,1}(D, K_{1,c}, 0) &= a_1(D - D^*), \quad c_{Z_a/Z_p,1} = r_{Z_a/Z_p,U_4,1} c_{U_4,1} \\
c_{U_4,2}(D, K_{1,c}, 0) &= b_1 \\
c_{Z_a/Z_p,3}(D, K_{1,c}, 0) &= d_1, \quad c_{U_4,3} = r_{U_4,Z_a/Z_p,3} c_{Z_a/Z_p,3}
\end{aligned} \tag{30}$$

and for $D \rightarrow \infty$:

$$\begin{aligned}
c_{U_4,1}(\infty, K_{1,c}, K_3) &= a_2(K_3 - K_3^*) + e_2(K_3 - K_3^*)^2, \quad c_{Z_a/Z_p,1} = r_{Z_a/Z_p,U_4,1} c_{U_4,1} \\
c_{U_4,2}(\infty, K_{1,c}, K_3) &= b_2 \\
c_{Z_a/Z_p,3}(\infty, K_{1,c}, K_3) &= d_2(K_3 - K_3^{iso}), \quad c_{U_4,3} = r_{U_4,Z_a/Z_p,3} c_{Z_a/Z_p,3}
\end{aligned} \tag{31}$$

In the fits, the free parameters are $K_{1,c}(D, K_3)$, R_i^* , D^* , K_3^* , K_3^{iso} , a_1 , a_2 , b_1 , b_2 , d_1 , d_2 , e_2 , $r_{Z_a/Z_p,U_4,1}$, and $r_{U_4,Z_a/Z_p,3}$. Fits with this parameterization are labeled by A. Note that based on the results of Ref. [13], the difference between $K_{1,c}(D, K_3 = 0)$ for $q = 8$ and 12, is small but clearly larger than the statistical error that we achieve here. Therefore, we use a free fit parameter for each value of q . For all other parameters of the fit, we expect that the difference is much smaller than the statistical error. Therefore joint fit parameters are used.

In a second parameterization, we have added a linear dependence of $c_{U_4,2}$ on D and K_3 , respectively. Fits with this parameterization are labeled by B.

For $j_{max} = 4$, we take four free parameters for the amplitudes $c_{Z_a/Z_p,4}$ and $c_{U_4,4}$ for $K_3 = 0$ and $D \rightarrow \infty$ in addition. Putting this on top of the parameterization A is denoted by AA below, while putting it on top of B is denoted by AB.

We fitted the data taking into account linear lattice sizes $L \geq L_{min}$. Typically, first $\chi/\text{D.O.F.}$ decreases rapidly, with increasing L_{min} and then levels off at $\chi/\text{D.O.F.} \approx 1$. The corresponding p -values reach an acceptable range. For $L_{min} \approx 13, 13, 9$, and 9 the levelling off is reached for the parameterizations A, B, AA, and AB, respectively. In the case of AA and BB, $\epsilon_4 = 3.6$ is used. For a discussion of $\chi/\text{D.O.F.}$ and the corresponding p -value see appendix A of Ref. [50]. Throughout this work, least square fits were performed by using the function `curve_fit()` contained in the SciPy library [51]. Plots were generated by using the Matplotlib library [52].

Our final estimates of R_i^* , D^* , K_3^* , K_3^{iso} , and $K_{1,c}(D, K_3)$, are obtained in the following way: We require that for each of the Ansätze, there is at least one L_{min} with an acceptable

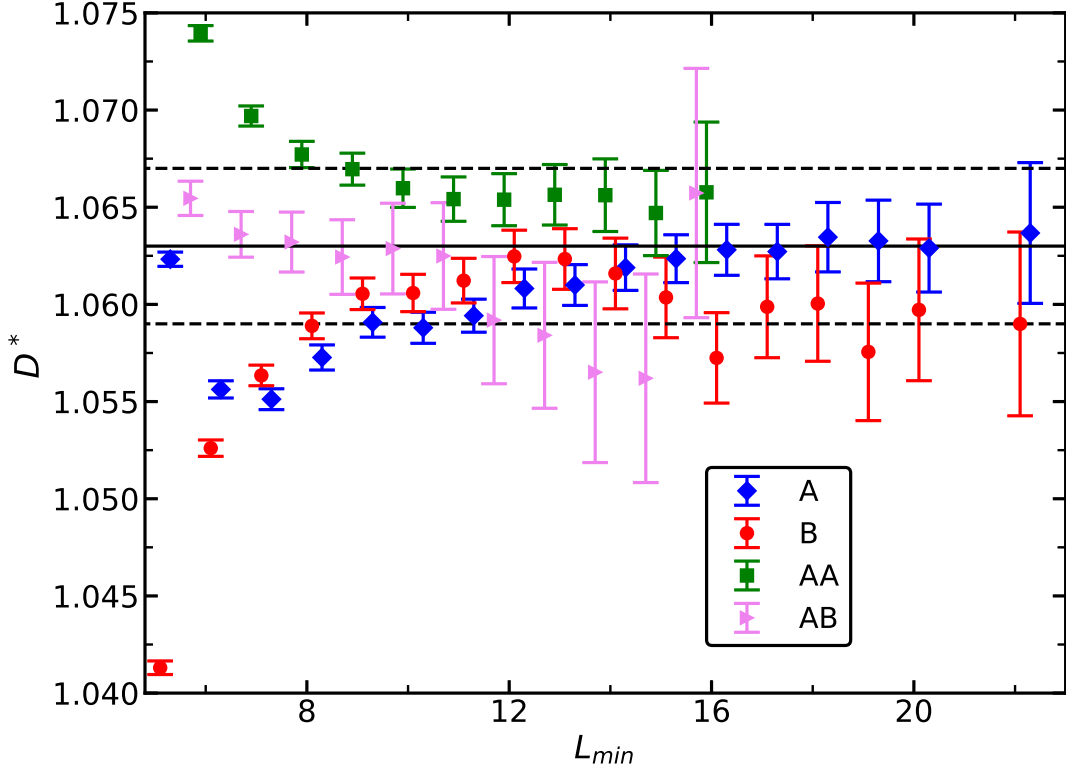


FIG. 2. We plot estimates of D^* for $K_3 = 0$ obtained by using four different Ansätze as function of L_{min} , where all data obtained for $L \geq L_{min}$ are taken into account in the fit. The Ansätze A, B, AA and AB are discussed in the text. The solid line gives our final estimate $D^* = 1.063$, while the dashed lines indicate our error estimate. Note that the values on the x -axis are slightly shifted to reduce overlap of the symbols.

p -value that gives an estimate consistent with the final estimate. In general, this way the error is larger than the error based on a single Ansatz. The variation of the estimate over different Ansätze provides an estimate of systematic errors. In Fig. 2 we plot estimates of D^* for $K_3 = 0$ as a function of L_{min} for the four Ansätze discussed above. In Figs. 3 and 4 we plot analogous data for K_3^* and K_3^{iso} at $D \rightarrow \infty$, respectively.

Our final estimates are

$$(Z_a/Z_p)^* = 0.320380(8) \quad (32)$$

$$U_4^* = 1.242934(10) \quad (33)$$

$$r_{Z_a/Z_p, U_4, 1} = -0.415(15) \quad (34)$$

$$D^* = 1.063(6) \quad (35)$$

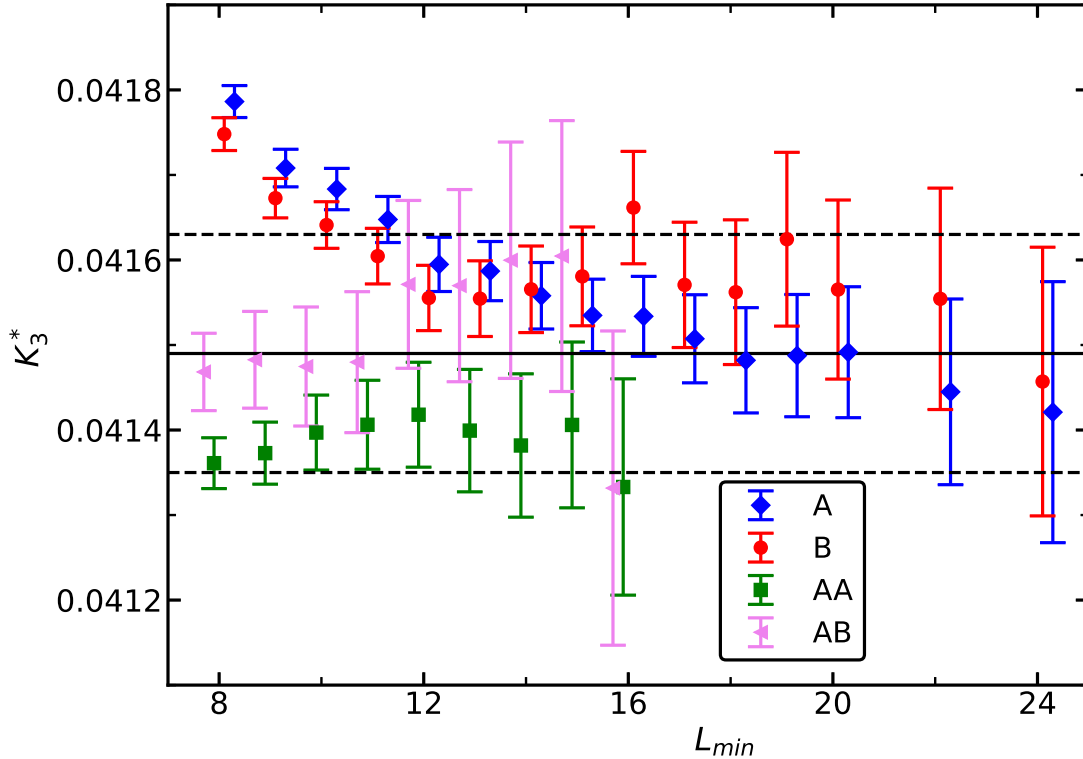


FIG. 3. We plot estimates of K_3^* for $D \rightarrow \infty$ obtained by using four different Ansätze as a function of L_{min} , where all data obtained for $L \geq L_{min}$ are taken into account in the fit. The Ansätze labelled by A , B , AA , and AB are discussed in the text. The solid line gives our final estimate, while the dashed lines indicate our preliminary error estimate. Note that the values on the x -axis are slightly shifted to reduce overlap of the symbols.

$$K_3^* = 0.04149(14) \quad (36)$$

$$K_3^{iso} = 0.0498(23) . \quad (37)$$

In terms of the ratio $r_K = K_3/K_1$ at criticality we get $r_K^* = 0.1119(5)$ and $r_K^{iso} = 0.140(8)$. The estimate of r_K^{iso} is consistent with Eq. (28) obtained above but less precise. Furthermore one should note that here K_3^{iso} highly relies on the fact that Z_a/Z_p , in contrast to U_4 , U_6 and ξ_{2nd}/L , is not affected by the analytic background of the magnetic susceptibility. Analyzing the numbers of table I and II, we find that the violation of the rotational invariance at r_K^* is reduced by a factor of about 9 compared with $r_K = 0$, which translates to a scale factor of a little bit less than 3. In terms of reduction of the volume this means a factor of about $3^3 = 27$.

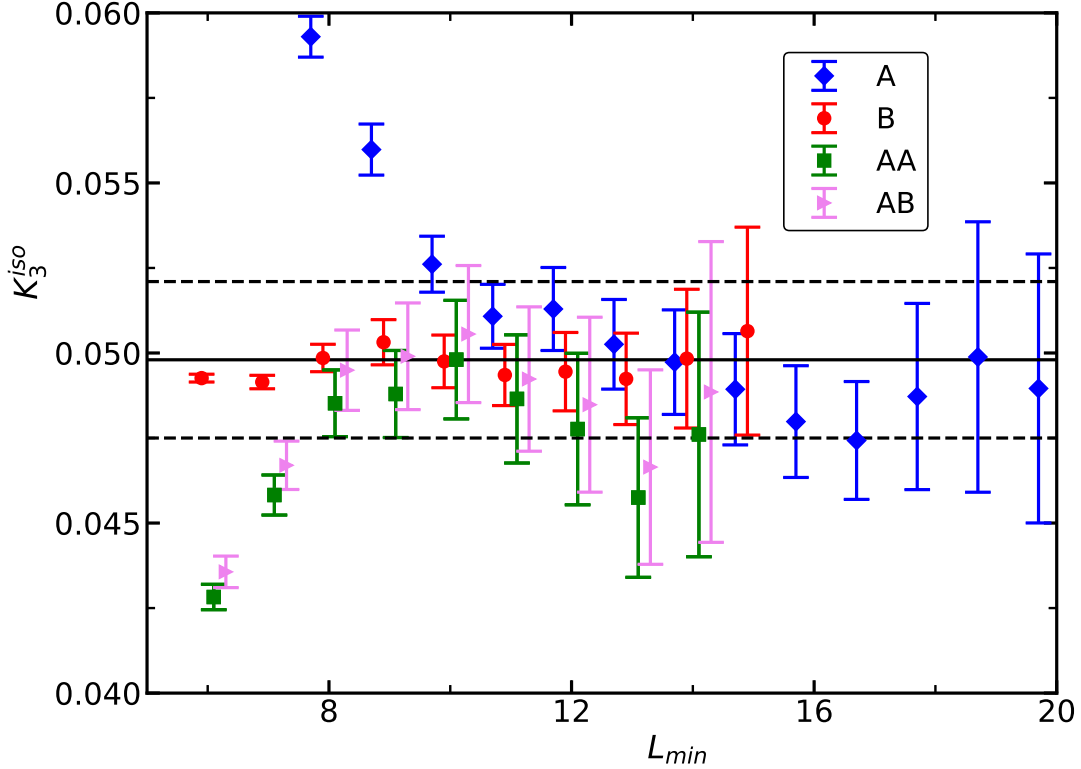


FIG. 4. We plot estimates of K_3^{iso} for $D \rightarrow \infty$ obtained by using four different Ansätze as a function of L_{min} , where all data obtained for $L \geq L_{min}$ are taken into account in the fit. The Ansätze labelled by A , B , AA , and AB are discussed in the text. The solid line gives our final estimate, while the dashed lines indicate our preliminary error estimate. Note that the values on the x -axis are slightly shifted to reduce overlap of the symbols.

Analyzing the data sets with ξ_{2nd}/L correctly measured gives us $\xi_{2nd}/L = 0.592363(12)$ and $U_6 = 1.75035(5)$. Furthermore $r_{\xi_{2nd}/L, U_4, 1} = 0.435(15)$ and $r_{U_6, U_4, 1} = 3.605(5)$. Estimates of the critical coupling $K_{1,c}$ are summarized in table III. The ratio of $K_{1,c}$, which is denoted by β_c in Ref. [13], for $q = 8$ and $q = 12$ at $D = 1.07$ in table VII of Ref. [13] is fully consistent with the one obtained here. Our results for the fixed point values of the dimensionless quantities are consistent with those given in Ref. [13]. The accuracy is clearly improved.

TABLE III. Estimates of the critical coupling $K_{1,c}$ for given D and K_3 .

| D | K_3 | $K_{1,c}$ |
|----------------|--------|-----------------|
| 1.02, $q = 8$ | 0 | 0.563796225(35) |
| 1.05, $q = 8$ | 0 | 0.560823902(25) |
| 1.05, $q = 12$ | 0 | 0.560824190(30) |
| 1.06, $q = 12$ | 0 | 0.559849876(22) |
| 1.07, $q = 8$ | 0 | 0.558883385(25) |
| 1.07, $q = 12$ | 0 | 0.558883648(30) |
| ∞ | 0.04 | 0.37360041(3) |
| ∞ | 0.0415 | 0.37069947(2) |
| ∞ | 0.042 | 0.36973446(3) |
| ∞ | 0.046 | 0.36204960(4) |
| ∞ | 0.05 | 0.35442761(4) |

D. The critical exponent η

At the critical point, the magnetic susceptibility behaves as

$$\chi = a(D, K_3)L^{2-\eta}[1 + c(D, K_3)L^{-\omega} + dc^2(D, K_3)L^{-2\omega} + \dots + e(D, K_3)L^{-\omega_{NR}} + \dots] + b(D, K_3), \quad (38)$$

where $b(D, K_3)$ is the analytic background of the magnetic susceptibility. For a derivation of this behavior see for example Sec. III B of Ref. [13]. Instead of computing the magnetic susceptibility at an estimate of $K_{1,c}$, we compute it at a fixed value of a dimensionless quantity. In particular, here we take it at $Z_a/Z_p = 0.32038$ or $\xi_{2nd}/L = 0.592363$.

Furthermore, we consider multiplying χ by a power of U_4 , such that the correction $cL^{-\omega}$ vanishes for any value of (D, K_3) . We have used $\chi_{imp} = \chi U_4^p$, where $p = -0.98(1)$ for fixing $Z_a/Z_p = 0.32038$ and $p = -0.45(1)$ for $\xi_{2nd}/L = 0.592363$. In the appendix A, we discuss how we extract these values from data for $q = 8$ and $K_3 = 0$ at $D = 0.9$ and $D = 1.24$ that were generated for Ref. [13]. Since p is universal, it applies to the model $D \rightarrow \infty$ and $K_3 > 0$ studied here. As check, we compare results for η obtained for χ and χ_{imp} at

$Z_a/Z_p = 0.32038$. These are obtained by using the Ansatz

$$\chi = aL^{2-\eta} + b. \quad (39)$$

In this Ansatz, we omit leading corrections. Hence we expect a dependence of the estimate of η on K_3 due the leading correction that depends on K_3 . Furthermore we omit subleading corrections. They are at least partially taken into account by the additive parameter b . The results for $L_{min} = 16$ for $K_3 > 0$ are shown in Fig. 5. Note that for $K_3 = 0.0415$ we get an acceptable p -value starting from $L_{min} = 10$. We find that for χ_{imp} the estimates of η obtained for different values of K_3 are consistent, while this is clearly not the case for χ . We see a significant increase of the estimate of η with increasing K_3 . For $K_3 = 0.0415$, the estimates obtained from χ_{imp} and χ are consistent as we expect for K_3^* . Note that for $K_3 = 0.05$, we get for example $\eta = 0.038709(14)$, $0.038660(21)$, $0.038631(31)$, and $0.038632(44)$, for $L_{min} = 16, 20, 24$, and 28 , respectively. Furthermore, $\chi^2/\text{DOF} = 1.890, 1.199, 0.771$, and 0.900 for these minimal linear lattice sizes that are included in the fit. One might be tempted to quote $\eta = 0.03863(5)$ as the final result. However the deviation from our final result or the estimate obtained by using the conformal bootstrap method [14] is about 9 times larger as this error estimate. This again reminds us that a χ^2/DOF close to one or an acceptable p -value of the fit says little about possible systematic errors in the parameters of the Ansatz that are due to corrections, which are not taken into account.

Our final estimate of η is based on fits of χ_{imp} at $\xi_{2nd}/L = 0.592363$ and $Z_a/Z_p = 0.32038$ at $K_3 = 0.0415$. Note that χ at a fixed value of Z_a/Z_p is less affected by corrections, while on the other hand, the statistical error of χ at a fixed value of ξ_{2nd}/L is considerably smaller than that of χ at a fixed value of Z_a/Z_p . Note that this observation is consistent with previous work [13, 44]. Hence it is a good cross check to analyze both these choices.

We used the Ansätze (39) and

$$\chi = aL^{2-\eta}(1 + cL^{-\omega_{NR}}) + b, \quad (40)$$

where we fix $\omega_{NR} = 2.02548$. In Fig. 6 the estimates of η are plotted versus the minimal lattice size L_{min} that is taken into account in the fit. In the caption of Fig. 6 we denote the data for fixing ξ_{2nd}/L by X and those for fixing Z_a/Z_p by Z. The number that follows, refers to the type of the Ansatz. For the Ansätze (39) and (40) there is 1 or 2, respectively. In the case of χ_{imp} at $\xi_{2nd}/L = 0.592363$ using the Ansatz (39) we get an acceptable p -value

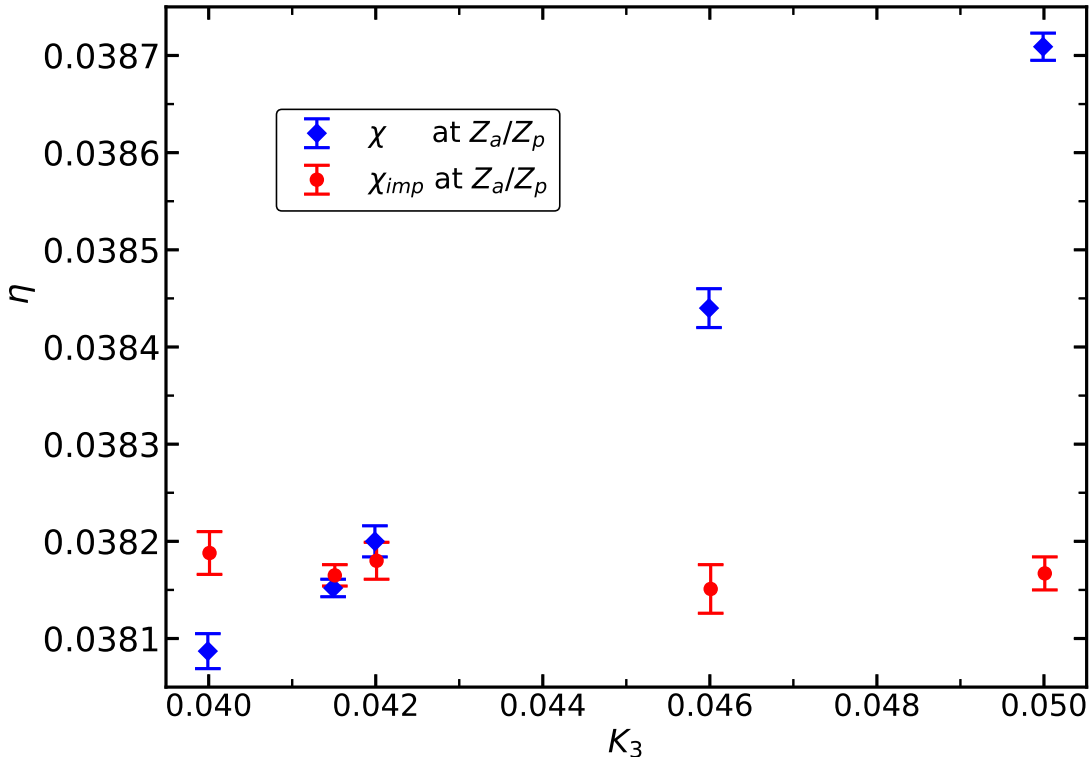


FIG. 5. We plot estimates of η obtained by using the Ansatz (39) for the model $D \rightarrow \infty$ and $K_3 > 0$ as a function of K_3 . Throughout, the minimal lattice size $L_{min} = 16$ is used. We give results obtained by fitting data for χ as well as χ_{imp} , both at $Z_a/Z_p = 0.32038$.

starting from $L_{min} = 20$. Still the estimate of η is increasing and it is not consistent with that obtained by the other fits. For the fit with Ansatz (40) we get an acceptable p -value already for $L_{min} = 8$. The same holds for χ_{imp} at $Z_a/Z_p = 0.32038$ using the Ansätze (39,40). Our final estimate is based on the fits Z1, Z2, and X2, since the estimates obtained by using X1 seem to converge much worse than those of the other three fits. In the case of Ansatz (40), one should note that replacing the numerical value $\omega_{NR} = 2.02548$ by for example 2, the estimates of η change only by little. Hence our estimate of η does not rely critically on the accurate determination of ω_{NR} by using the CB method. Our final estimate

$$\eta = 0.03816(2) \tag{41}$$

is chosen such that estimates for some L_{min} for each of Z1, Z2, and X2 are contained in the error bar. Note that this estimate is consistent with $\eta = 0.038176(44)$ obtained by using the conformal bootstrap method [14]. The error is considerably reduced compared with our

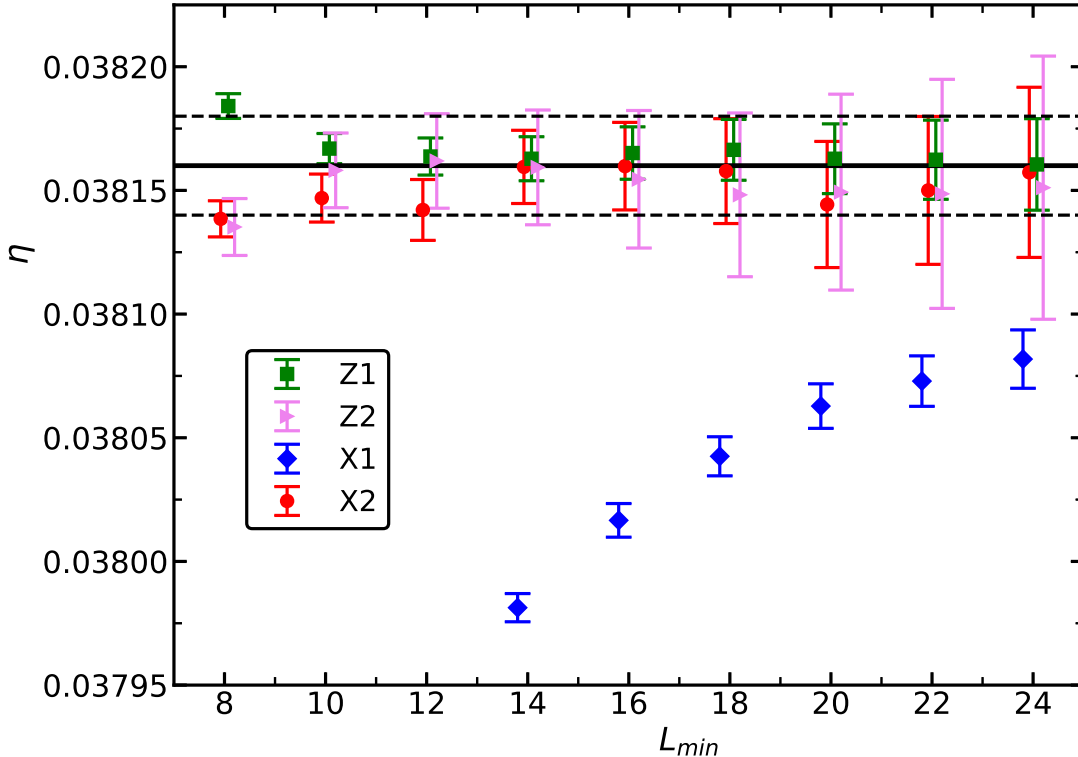


FIG. 6. We plot estimates of η obtained by fitting data for the improved magnetic susceptibility χ_{imp} for $(D, K_3) = (\infty, 0.0415)$. For a discussion of the fits see the text. The solid line gives our final estimate, while the dashed lines indicate our error estimate. Note that the values on the x -axis are slightly shifted to reduce overlap of the symbols.

previous estimate $\eta = 0.03810(8)$ [13].

As a consistency check, we analyzed our data for $(D, K_3) = (1.06, 0)$ in a similar fashion. Note that here we have used less CPU time than for $(D, K_3) = (\infty, 0.0415)$ and the maximal lattice size that we have simulated is $L_{max} = 100$ instead of 200. Our numerical estimates are given in Fig. 7, which is analogous to Fig. 6. The numerical estimates of η are fully compatible with the final estimate given in Eq. (41). However, one arrives at an error bar that is about three times as large.

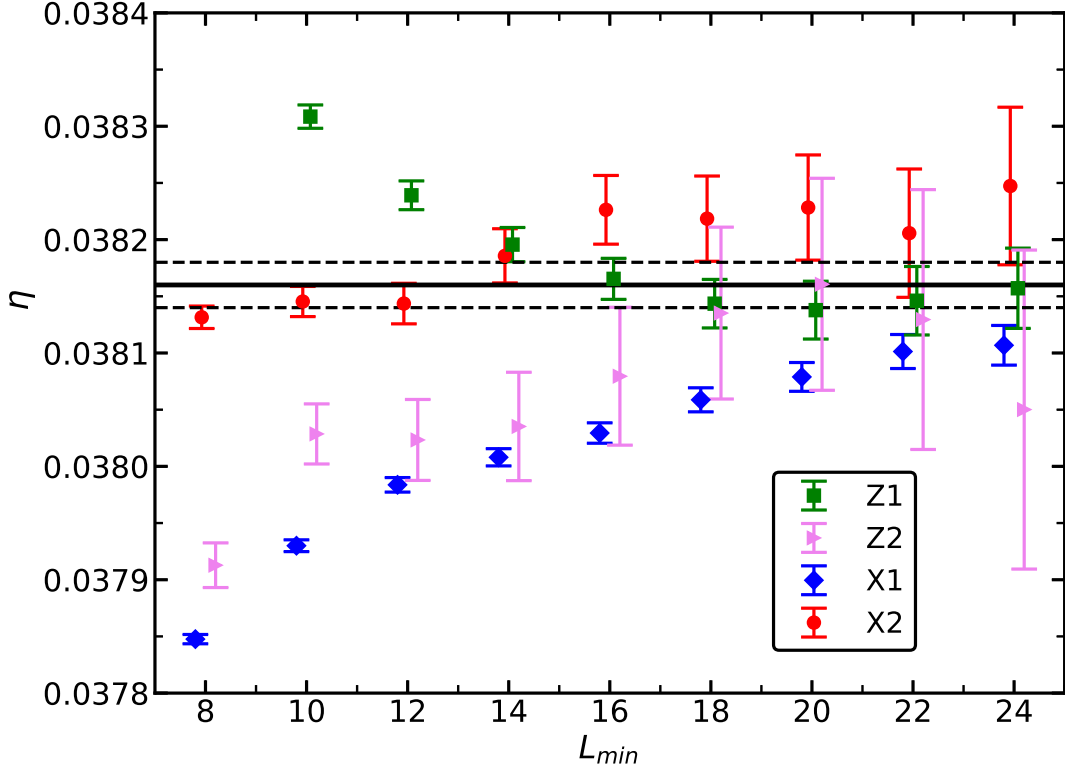


FIG. 7. We plot estimates of η obtained by fitting data for the improved magnetic susceptibility χ_{imp} at $(D, K_3) = (1.06, 0)$. For comparison we give our final estimate obtained by analyzing the data for $(D, K_3) = (\infty, 0.0415)$ as solid line. The dashed lines indicate the error of this estimate. Note that the values on the x -axis are slightly shifted to reduce overlap of the symbols.

E. The thermal RG exponent y_t

The thermal RG exponent is extracted from the behavior of the slopes of dimensionless quantities at criticality. In general we expect

$$\begin{aligned}
 S = & a(D, K_3)L^{y_t} [1 + b(D, K_3)L^{-\omega} + cb^2(D, K_3)L^{-2\omega} + \dots \\
 & + f(D, K_3)L^{-2+\eta} + d(D, K_3)L^{-\omega_{NR}} + \dots] + e(D, K_3)L^{-\omega} + \dots . \quad (42)
 \end{aligned}$$

For a derivation of this behavior see for example Sec. III C of Ref. [13]. The term $f(D, K_3)L^{-2+\eta}$ originates from the analytic background of the magnetic susceptibility. It is present for U_4 , U_6 , ξ_{2nd}/L , but not for Z_a/Z_p . Therefore we give preference to Z_a/Z_p estimating y_t . Note that the term $e(D, K_3)L^{-\omega}$ originates from the partial derivative of the dimensionless quantity R with respect to the scaling field of the leading correction. Effec-

tively it amounts to a correction with the correction exponent $y_t + \omega \approx 2.28$, which is only somewhat larger than ω_{NR} .

Using the results of section VC we can construct linear combinations of dimensionless quantities that do not depend on this scaling field. Here we shall analyze the slope of $Z_a/Z_p - c_{Z_a/Z_p, U_4} U_4$, where the numerical value of the coefficient is taken from Eq. (34).

In a preliminary step, for $D \rightarrow \infty$, we compute an estimate of y_t for each value of K_3 separately. To this end, we fit the data by using the Ansatz

$$S = aL^{y_t} (1 + bL^{-\epsilon}), \quad (43)$$

where we take $\epsilon = \omega_{NR} = 2.02548$. Similar to the preliminary analysis of the magnetic susceptibility, we compare the estimates obtained for $S_{Z_a/Z_p, imp}$ and S_{Z_a/Z_p} both at $Z_a/Z_p = 0.32038$. The improved slope is obtained by using the exponent $p = 0.92(4)$. In Fig. 8 we give results obtained for $L_{min} = 16$ for all values of K_3 studied here. Qualitatively, we see a similar behavior as for the estimates of η . In the case of S_{Z_a/Z_p} we see a dependence of the estimate of ν on K_3 , while this is not the case for $S_{Z_a/Z_p, imp}$. However this effect is less pronounced than in the case of η , studied above.

Next we focus on $K_3 = 0.0415$, which is close to K_3^* , and where we have accumulated the highest statistics and reached the largest linear lattice size simulated in this study. Also here, we used the Ansatz (43). In Fig. 9 we plot estimates of y_t as a function of L_{min} obtained for S_{Z_a/Z_p} (B), $S_{Z_a/Z_p, imp}$ (I), $S_{Z_a/Z_p - c_{Z_a/Z_p, U_4} U_4}$ (BSUM), and $S_{Z_a/Z_p - c_{Z_a/Z_p, U_4} U_4, imp}$ (ISUM), all taken at $Z_a/Z_p = 0.32038$. The improved slope $S_{Z_a/Z_p - c_{Z_a/Z_p, U_4} U_4, imp}$ is obtained by using the exponent $p = 0.22(4)$. The short names B, I, BSUM, and ISUM are used in the caption. The results shown in Fig. 9 are obtained by using $\epsilon = 2.02548$ in the Ansatz (43). We have checked that the results change only slightly when using $\epsilon = 2 - \eta$ instead.

These different slopes should be affected by corrections not fully taken into account in the Ansatz in different ways:

- B: small corrections $\propto L^{-\omega}$, corrections $\propto L^{-y_t - \omega}$.
- I: very small corrections $\propto L^{-\omega}$, corrections $\propto L^{-2+\eta}$, corrections $\propto L^{-y_t - \omega}$.
- BSUM: small corrections $\propto L^{-\omega}$, corrections $\propto L^{-2+\eta}$, small corrections $\propto L^{-y_t - \omega}$.
- ISUM: very small corrections $\propto L^{-\omega}$, corrections $\propto L^{-2+\eta}$, small corrections $\propto L^{-y_t - \omega}$.

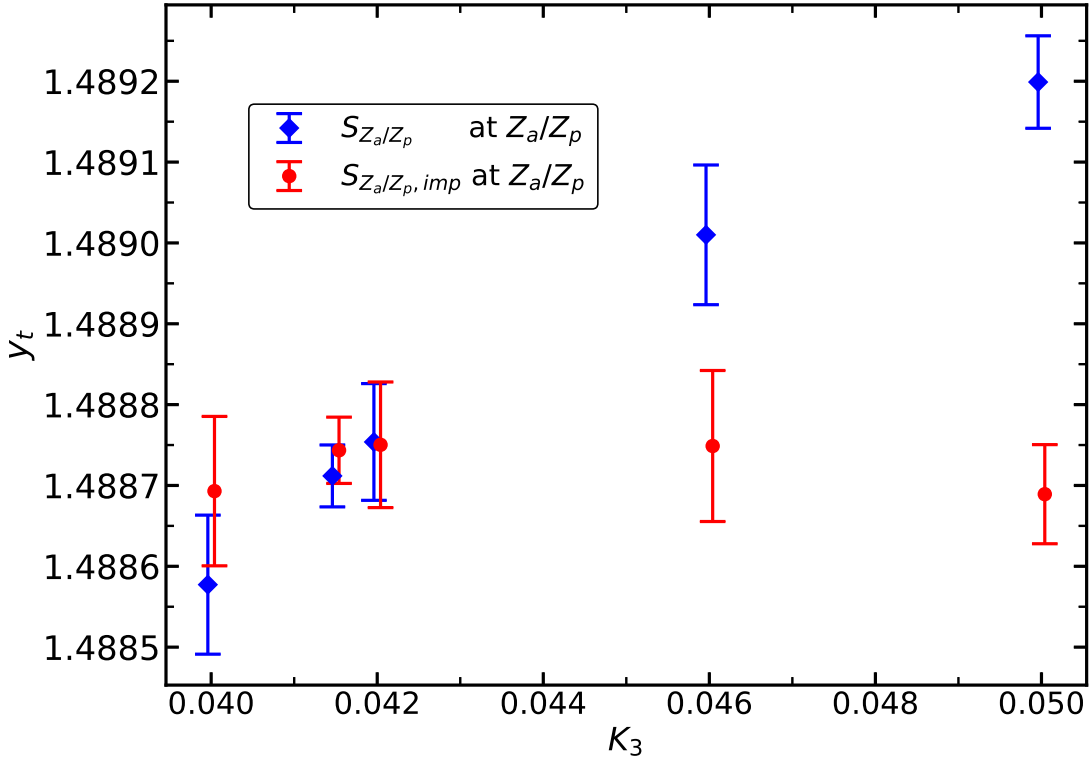


FIG. 8. We plot estimates of y_t obtained by using the Ansatz (43) for the model $D \rightarrow \infty$ and $K_3 > 0$ as a function of K_3 . Throughout, the minimal lattice size $L_{min} = 16$ is used. We give results obtained by fitting data for S_{Z_a/Z_p} as well as $S_{Z_a/Z_p, imp}$, both at $Z_a/Z_p = 0.32038$, using the Ansatz (43).

Therefore the spread of the results should indicate the size of the systematic errors. Assuming that the spectrum of operators looks similar as for the Ising universality class, $\omega_i \gtrsim 3.4$ for corrections not discussed above.

The solid line in Fig. 9 gives our final result for y_t and the dashed lines give the error. The error is chosen such that for each of the four fits there is at least one L_{min} with an acceptable p -value that gives a consistent estimate. In the appendix A of Ref. [50] we discuss in more detail how we arrive at final results and their error. Here we obtain

$$y_t = 1.48872(5) , \quad (44)$$

which is consistent but more precise than our previous estimate $y_t = 1.48879(14)$ [13]. CB [14] gives $y_t = 3 - 1.51136(22) = 1.48864(22)$. For a more comprehensive comparison with the literature see Sec. VI below.

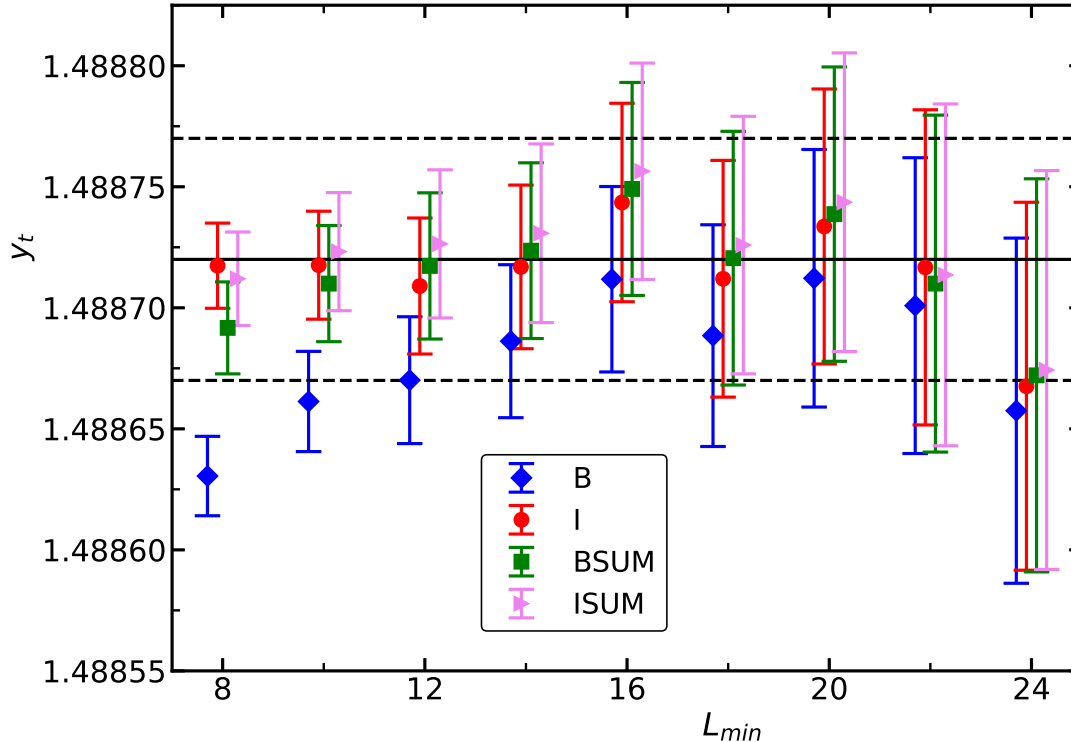


FIG. 9. We plot estimates of y_t obtained by using the Ansatz (43) versus the minimal lattice size that is included into the fit. Only data taken at $K_3 = 0.0415$ are used. Four different slopes are analyzed. Details and the meaning of B, I, BSUM, and ISUM are discussed in the text. The solid line gives our final estimate, while the dashed lines indicate our error estimate. Note that the values on the x -axis are slightly shifted to reduce overlap of the symbols.

As check, we analyzed the slopes of U_4 and ξ_{2nd}/L . We get consistent but less accurate results. The same holds for analyzing the data for $(D, K_3) = (1.06, 0)$. We abstain from a detailed discussion.

VI. SUMMARY AND CONCLUSIONS

We further advance the programme of improved lattice models. The basic idea of improved models is that a parameter of the reduced Hamiltonian is tuned such that the leading correction to scaling vanishes. This approach has to be contrasted with efforts to construct perfect actions (reduced Hamiltonians) as it was proposed in Ref. [53] for example. For a discussion of improved models, where one parameter is tuned see for example Sec. 2.3

of the review [5]. The success of improved models relies on the fact that the spectrum of correction exponents is sparse at least for the leading corrections. The aim of studying improved models is to obtain accurate results for universal quantities. Recent applications to the Ising, XY , Heisenberg and $O(4)$ -invariant universality classes in three dimensions are Refs. [13, 54–56]. In these cases $\omega \approx 0.8$. For the diluted Ising universality class the correction exponent is $\omega = 0.33(3)$ [57]. In this case it is virtually mandatory to simulate at the optimal dilution parameter to obtain accurate estimates of the critical exponents. In general, the smaller the correction exponent, the more important is the improvement to obtain accurate estimates of universal quantities. A natural question is whether the program can be extended to more than one correction. Recently we have studied the $O(N)$ -invariant ϕ^4 model in three dimensions with a perturbation that has only cubic symmetry for $N = 3$ and 4. Here $\omega_1 = 0.763(24)$ and $\omega_2 = 0.082(5)$ for $N = 4$ and $\omega_2 = 0.0133(8)$ for $N = 3$ [50, 58] for the cubic fixed point. In the case of $N = 3$ it is plausible that the value of ω_1 is very close to $\omega = 0.759(2)$ [55] for the $O(3)$ -invariant fixed point. Note that the choice of the subscript of ω follows the literature. Here it is virtually impossible to obtain accurate results for the critical exponents of the cubic fixed point without improvement of the reduced Hamiltonian. In Refs. [50, 58] we eliminate the two leading corrections by tuning two parameters of the reduced Hamiltonian.

In Ref. [8] we study the Blume-Capel model on the simple cubic lattice with next-to-next-to-nearest neighbor interactions in addition to nearest neighbor interactions. Essentially by tuning the ratio of the corresponding couplings K_3/K_1 , we eliminate the leading violation of spatial rotational invariance, while the leading correction is eliminated by additionally tuning the dynamic dilution, or crystal field, parameter D . Highly accurate estimates of critical exponents for the Ising universality class were obtained.

In the present work we investigate whether this approach can be applied successfully in the case of the XY universality class. We build on a preliminary study presented in the appendix of Ref. [8]. We find that in a rigorous sense this is not the case. However for $D \rightarrow \infty$, leading corrections are eliminated for $(K_3/K_1)^* = 0.1119(5)$, where the spatial unisotropy is reduced by a factor of about 9 compared with the model at $K_3 = 0$. The price to pay for $K_3 > 0$ is the excess CPU time needed compared with the q -state clock model with nearest neighbor couplings only. The q -state clock model can be simulated by using the single cluster algorithm [7] only. The main task in the algorithm is to check, whether a link

to the nearest neighbor, and here in addition the next-to-next-to-nearest neighbor, is frozen or not. Since there are six nearest neighbors and eight next-to-next-to-nearest neighbors, we naively expect that the CPU time needed increases by the factor $(6 + 8)/6 = 2.3\dots$. Comparing our own implementations of the update, we see a factor slightly smaller than two.

At $K_3 = 0.0415$, which is close to K_3^* , we performed high statistics simulations on lattices with a linear lattice size up to $L = 200$. A FSS analysis of the data provided us with accurate estimates of the critical exponents η and $y_t = 1/\nu$. In table IV our results are compared with ones given in the literature. These were obtained by using various theoretical methods and experiments. In particular in the case of field theoretic methods it is virtually impossible to give a complete overview on the vast literature.

The ϵ -expansion has been introduced in Ref. [59], where the leading order result is given. The expansion parameter is $\epsilon = 4 - d$, where d is the dimension of the system. Over the years, coefficients for higher orders were computed. For an account see table 3 of Ref. [26]. It turns out that the series is divergent and in order to obtain a numerical result for the critical exponents in three dimensions resummation of the series is required. Various methods have been applied to this end. In general the systematic error is hard to estimate and hence the error that is quoted depends on the judgment of the authors. In table IV we give a small selection of results. The precision is clearly less than that obtained here or by using CB. The same holds for the results of the expansion in three dimensions fixed [20] and FRG [36]. For more field theoretical results see table 19 of Ref. [5].

Lattice models can be studied by various methods. Precise estimates of critical exponents of three-dimensional systems are obtained by analyzing high temperature series expansions or Monte Carlo simulations. In Ref. [60] the high temperature series of the susceptibility and the correlation length were computed up to the order β^{21} , where β is the inverse temperature, for $O(N)$ -invariant nonlinear σ models on the simple cubic and the body centered cubic lattice. Numerical results for the exponents γ and ν are given in table II of Ref. [60]. In table IV we give estimates for $N = 2$, where we compute $\eta = 2 - \gamma/\nu$. We abstain from quoting an error for η , since it is unclear how γ and ν are correlated. For previous work see Ref. [60].

An early Monte Carlo study of the XY model on the simple cubic lattice is Ref. [61]. Using the Monte Carlo renormalization group (MCRG), estimates of the RG exponents y_h

and y_t were computed. However no final estimate is quoted. It is interesting to note that in addition to the standard XY model an improved model is simulated. In addition to the nearest neighbor coupling a second term, Eq. (11) of Ref. [61], is added in the Hamiltonian. For a discussion see sec. IV. of Ref. [61]. The advent of the cluster algorithm [6, 7] was a milestone in the simulation of $O(N)$ -invariant lattice models. This can be clearly seen when comparing the results of Ref. [62] with [23]. In Ref. [62], where the single cluster algorithm has been used, much more precise estimates are obtained than in Ref. [23], where a local algorithm had been employed. In Refs. [13, 21, 25, 63] improved models were simulated by using cluster algorithms. In Refs. [21, 25] the most accurate estimates of the critical exponents are actually obtained from the analysis of high temperature series. The analysis is biased by using the estimates of λ^* , D^* and β_c obtained from Monte Carlo simulations in combination with FSS. Note that λ is the parameter of the ϕ^4 model that has been studied in Refs. [21, 25]. In Ref. [22] two classical models and a quantum model are simulated using worm-type algorithms.

Let us turn to experiments. In Ref. [64] the λ -transition of ^4He has been studied. The exponent ν has been determined from the behavior of the superfluid fraction, which is obtained from the second sound velocity. This estimate is fully consistent with recent theoretical results. In Refs. [17–19] the specific heat in the neighborhood of the λ -transition has been measured on a Spacelab mission, avoiding gravitational rounding of the transition. The final analysis of the data provided the estimate $\alpha = -0.0127(3)$, which is converted in table IV by using the hyperscaling relation $\nu = (2 - \alpha)/d$. The deviation of this result from recent theoretical estimates is 8 times larger than the error that is quoted. Phase transitions in the XY universality class are also expected for other materials. For example magnets with an easy axis. A more recent experiment on CsMnF_3 , where the specific heat (C) and the thermal diffusivity (D) have been measured, is reported in Ref. [66]. In addition, data from Ref. [65] for the specific heat of SmMnO_3 have been analyzed in [66]. These results are quite accurate and more or less agree with the theoretical one. For more experimental results see table 20 of Ref. [5].

The estimates obtained here could be improved simply by spending more CPU time to get better statistics and larger lattice sizes. Performing high temperature series expansions for the q -state clock model with nearest and next-to-next-to-nearest neighbor couplings might also allow to further improve the accuracy of critical exponents. The estimates of K_3^* and

TABLE IV. We summarize estimates of critical exponents of the three-dimensional XY universality class. MC: Monte Carlo simulation of lattice models. HT: Analysis of high temperature series of lattice models. FRG: functional renormalization group. CB: conformal bootstrap. * means that the exponent is not directly given in the cited paper. For a discussion see the text.

| method | year | Ref. | ν | η | ω |
|----------------------------|----------------|----------|---------------|--------------|-----------|
| 3D-exp | 1998 | [20] | 0.6703(15) | 0.0354(25) | 0.789(11) |
| ϵ 5-loop | 1998 | [20] | 0.6680(35) | 0.0380(50) | 0.802(18) |
| ϵ 6-loop | 2017 | [67] | 0.6690(10) | 0.0380(6) | 0.804(3) |
| ϵ 7-loop | 2021 | [68, 69] | 0.67076(38) | 0.03810(56) | 0.789(13) |
| FRG | 2020 | [36] | 0.6716(6) | 0.0380(13) | 0.791(8) |
| CB | 2016 | [9] | 0.6719(12) | 0.0385(7) | 0.811(19) |
| CB | 2019 | [14] | 0.671754(100) | 0.038176(44) | 0.794(8) |
| HT, sc | 1997 | [60] | 0.677(3) | 0.0399* | - |
| HT, bcc | 1997 | [60] | 0.674(2) | 0.0386* | - |
| MC | 1989 | [23] | 0.67(2) | 0.075* | - |
| MC | 1990 | [62] | 0.670(2) | 0.036(14) | - |
| MC | 1999 | [63] | 0.6723(3)[8] | 0.0381(2)[2] | 0.79(2) |
| MC+HT | 2001 | [25] | 0.67155(27) | 0.0380(4) | - |
| MC+HT | 2006 | [21] | 0.6717(1) | 0.0381(2) | 0.785(20) |
| MC | 2019 | [22] | 0.67183(18) | 0.03853(48) | 0.77(13) |
| MC | 2019 | [13] | 0.67169(7) | 0.03810(8) | 0.789(4) |
| MC | 2025 this work | | 0.671718(23) | 0.03816(2) | - |
| ^4He | 1984 | [64] | 0.6717(4) | - | - |
| ^4He | 2003 | [17–19] | 0.6709(1) | - | - |
| SmMnO_3, C | 2012 | [65, 66] | 0.6710(3) | - | - |
| CsMnF_3, D | 2014 | [66] | 0.6710(7) | - | - |
| CsMnF_3, C | 2014 | [66] | 0.6720(13) | - | - |

$K_{1,c}$ obtained here could be used to bias the analysis of the series.

The model studied here could be used to study universal amplitude ratios, critical dynamical behavior, and the physics of boundaries and thin films in the neighborhood of the critical temperature.

VII. ACKNOWLEDGEMENT

I like to thank Slava Rychkov for pointing my attention to refs. [26, 37] and Junyu Liu and David Simmons-Duffin for communicating the numerical value of ω_{NR} . This work was supported by the DFG under the grants No HA 3150/5-3 and HA 3150/5-4.

Appendix A: Improved observables

We eliminate leading corrections in the magnetic susceptibility and the slopes of dimensionless quantities by multiplying with a power p of U_4 . This idea goes back to Refs. [21, 57].

Simulating improved models, these quantities are useful, since D^* or K_3^* are only known approximately.

Let us discuss the method at the example of a slope, say at a fixed value of Z_a/Z_p :

$$\begin{aligned} S &= aL^{y_t}(1 + c_s L^{-\omega}) \\ U_4 &= U_4^*(1 + c_U L^{-\omega}), \end{aligned} \tag{A1}$$

where we only give the leading correction. We intent to construct

$$S_{imp} = SU_4^p = aU_4^{*,p}L^{y_t}(1 + c_s L^{-\omega})(1 + pc_U L^{-\omega} + \dots) = aU_4^{*,p}L^{y_t}(1 + [c_s + pc_U]L^{-\omega} + \dots) \tag{A2}$$

such that leading corrections vanish. Hence $p = -c_s/c_U$. In order to get estimates of c_s and c_U , one could perform simulations at values of D or K_3 , where leading corrections to scaling have a large amplitude and then fit the data by using Eqs. (A1) as Ansätze. However it is favorable to eliminate RG exponents first. To this end we consider a pair of parameters, where the leading corrections have opposite sign and roughly the same absolute value. To this end, we take data from simulations performed for [13] for the $(8 + 1)$ -state clock model at $D = 0.9$ and 1.24 . Computing the ratio

$$r_S(L) = \frac{S(L, D = 0.9)}{S(L, D = 1.24)} \tag{A3}$$

we eliminate L^y . Analogously $r_U(L) = U_4(L, D = 0.9)/U_4(L, D = 1.24)$, We perform fits by using the Ansatz

$$r_S(L) = \bar{a}r_U(L)^{-p}, \quad (\text{A4})$$

where \bar{a} and p are the free parameters of the fit. Note that in this Ansatz ω does not appear. In the fit we ignore the statistical error of $r_U(L)$, since its relative error is much smaller than that of $r_S(L)$. For $D = 0.9$ and $D = 1.24$, we had simulated lattices of a linear size up to $L = 48$. The estimates of p that we obtain are given in the main text.

-
- [1] K. G. Wilson and J. Kogut, *The renormalization group and the ϵ -expansion*, Phys. Rep. C **12**, 75 (1974).
 - [2] M. E. Fisher, *The renormalization group in the theory of critical behavior*, Rev. Mod. Phys. **46**, 597 (1974), Erratum: Rev. Mod. Phys. **47**, 543 (1975).
 - [3] John Cardy, *Scaling and Renormalization in Statistical Physics*, Series: Cambridge Lecture Notes in Physics (No. 5) (Cambridge University Press, Cambridge, 1996)
 - [4] M. E. Fisher, *Renormalization group theory: Its basis and formulation in statistical physics*, Rev. Mod. Phys. **70**, 653 (1998).
 - [5] A. Pelissetto and E. Vicari, *Critical Phenomena and Renormalization-Group Theory*, [arXiv:cond-mat/0012164], Phys. Rept. **368**, 549 (2002).
 - [6] Robert H. Swendsen and Jian-Sheng Wang, *Nonuniversal critical dynamics in Monte Carlo simulations*, Phys. Rev. Lett. **58**, 86 (1987).
 - [7] U. Wolff, *Collective Monte Carlo Updating for Spin Systems*, Phys. Rev. Lett. **62**, 361 (1989).
 - [8] Martin Hasenbusch, *Restoring isotropy in a three-dimensional lattice model: The Ising universality class*, [arXiv:2105.09781], Phys. Rev. B **104**, 014426 (2021).
 - [9] F. Kos, D. Poland, D. Simmons-Duffin, and A. Vichi, *Precision Islands in the Ising and $O(N)$ Models*, [arXiv:1603.04436], J. High Energ. Phys. 08 (2016), 36.
 - [10] D. Simmons-Duffin, *The Lightcone Bootstrap and the Spectrum of the 3d Ising CFT*, [arXiv:1612.08471], J. High Energ. Phys. 03 (2017), 86.
 - [11] M. Reehorst, *Rigorous bounds on irrelevant operators in the 3d Ising model CFT*, [arXiv:2111.12093] J. High Energ. Phys. 09 (2022), 177.
 - [12] Cyuan-Han Chang, Vasiliy Dommès, Rajeev S. Erramilli, Alexandre Homrich, Petr Kravchuk,

- Aike Liu, Matthew S. Mitchell, David Poland, David Simmons-Duffin, *Bootstrapping the 3d Ising Stress Tensor*, [arXiv:2411.15300], J. High Energ. Phys. 03 (2025), 136.
- [13] M. Hasenbusch, *Monte Carlo study of an improved clock model in three dimensions*, [arXiv:1910.05916], Phys. Rev. B **100**, 224517 (2019).
- [14] S. M. Chester, W. Landry, J. Liu, D. Poland, D. Simmons-Duffin, N. Su, and A. Vichi, *Carving out OPE space and precise $O(2)$ model critical exponents*, [arXiv:1912.03324], J. High Energ. Phys. 06 (2020), 142.
- [15] D. Poland, S. Rychkov, and A. Vichi, *The Conformal Bootstrap: Theory, Numerical Techniques, and Applications*, [arXiv:1805.04405], Rev. Mod. Phys. **91**, 15002 (2019).
- [16] Slava Rychkov and Ning Su, *New Developments in the Numerical Conformal Bootstrap*, [arXiv:2311.15844], Rev. Mod. Phys. **96**, 045004 (2024).
- [17] J. A. Lipa, D. R. Swanson, J. A. Nissen, T. C. P. Chui, and U. E. Israelsson, *Heat Capacity and Thermal Relaxation of Bulk Helium very near the Lambda Point*, Phys. Rev. Lett. **76**, 944 (1996).
- [18] J. A. Lipa, D. R. Swanson, J. A. Nissen, Z. K. Geng, P. R. Williamson, D. A. Stricker, T. C. P. Chui, U. E. Israelsson, and M. Larson, *Specific Heat of Helium Confined to a 57- μm Planar Geometry*, Phys. Rev. Lett. **84**, 4894 (2000).
- [19] J. A. Lipa, J. A. Nissen, D. A. Stricker, D. R. Swanson and T. C. P. Chui, *Specific heat of liquid helium in zero gravity very near the λ -point*, [arXiv:cond-mat/0310163], Phys. Rev. B **68**, 174518 (2003).
- [20] R. Guida and J. Zinn-Justin, *Critical exponents of the N vector model*, [arXiv:cond-mat/9803240], J. Phys. A **31**, 8103 (1998).
- [21] M. Campostrini, M. Hasenbusch, A. Pelissetto, and E. Vicari, *The critical exponents of the superfluid transition in He4*, [cond-mat/0605083], published as *Theoretical estimates of the critical exponents of the superfluid transition in He4 by lattice methods*, Phys. Rev. B **74**, 144506 (2006).
- [22] Wanwan Xu, Yanan Sun, Jian-Ping Lv, and Youjin Deng, *High-precision Monte Carlo study of several models in the three-dimensional $U(1)$ universality class*, [arXiv:1908.10990], Phys. Rev. B **100**, 064525 (2019).
- [23] Ying-Hong Li and S. Teitel, *Finite-size scaling study of the three-dimensional classical XY*

- model*, Phys. Rev. B **40**, 9122 (1989).
- [24] Yukihiro Komura and Yutaka Okabe, *CUDA programs for GPU computing of Swendsen-Wang multi-cluster spin flip algorithm: 2D and 3D Ising, Potts, and XY models*, [arXiv:1403.7560], Computer Physics Communications 185 (2014) 1038.
- [25] M. Campostrini, M. Hasenbusch, A. Pelissetto, P. Rossi, and E. Vicari, *Critical behavior of the three-dimensional XY universality class*, [cond-mat/0010360], Phys. Rev. B **63**, 214503 (2001).
- [26] Johan Henriksson, *The critical $O(N)$ CFT: Methods and conformal data*, [arXiv:2201.09520], Physics Reports **1002**, 1 (2023).
- [27] David R. Nelson, *Coexistence-curve singularities in isotropic ferromagnets*, Phys. Rev. B **13**, 2222 (1976).
- [28] Daniel J. Amit and Luca Peliti, *On dangerous irrelevant operators*, Annals of Physics **140**, 207 (1982).
- [29] L. Alvarez-Gaume, O. Loukas, D. Orlando, and S. Reffert, *Compensating strong coupling with large charge*, [arXiv:1610.04495], J. High Energ. Phys. 04 (2017), 059.
- [30] D. Banerjee, S. Chandrasekharan, and D. Orlando, *Conformal dimensions via large charge expansion*, [arXiv:1707.00711], Phys. Rev. Lett. **120**, 061603 (2018).
- [31] Gabriel Cuomo, J. M. Viana Parente Lopes, José Matos, Júlio Oliveira, and João Penedones, *Numerical tests of the large charge expansion*, [arXiv:2305.00499], J. High Energ. Phys. 05 (2024), 161.
- [32] M. Hasenbusch and E. Vicari, *Anisotropic perturbations in three-dimensional $O(N)$ -symmetric vector models*, [arXiv:1108.0491], Phys. Rev. B **84**, 125136 (2011).
- [33] J. Hove and A. Sudbø, *Criticality versus q in the $(2 + 1)$ -dimensional Z_q clock model*, [arXiv:cond-mat/0301499], Phys. Rev. E **68**, 046107 (2003).
- [34] H. Shao, W. Guo, and A. W. Sandvik, *Monte Carlo Renormalization Flows in the Space of Relevant and Irrelevant Operators: Application to Three-Dimensional Clock Models*, [arXiv:1905.13640], Phys. Rev. Lett. **124**, 080602 (2020).
- [35] Wei Zhu, Chao Han, Emilie Huffman, Johannes S. Hofmann, and Yin-Chen He, *Uncovering conformal symmetry in the 3D Ising transition: State-operator correspondence from a fuzzy sphere regularization*, [arXiv:2210.13482], Phys. Rev. X **13**, 021009 (2023).
- [36] G. De Polsi, I. Balog, M. Tissier, and N. Wschebor, *Precision calculation of critical ex-*

- ponents in the $O(N)$ universality classes with the nonperturbative renormalization group, [arXiv:2001.07525], Phys. Rev. E **101**, 042113 (2020).
- [37] Junyu Liu, David Meltzer, David Poland, David Simmons-Duffin, *The Lorentzian inversion formula and the spectrum of the 3d $O(2)$ CFT* [arXiv:2007.07914], J. High Energ. Phys. 09 (2020), 115.
- [38] Junyu Liu and David Simmons-Duffin, private communication.
- [39] A. N. Manashov, E. D. Skvortsov and M. Strohmaier, *Higher spin currents in the critical $O(N)$ vector model at $1/N^2$* , [arXiv:1706.09256], J. High Energ. Phys. 08 (2017), 106.
- [40] S. E. Derkachov, J. A. Gracey and A. N. Manashov, *Four loop anomalous dimensions of gradient operators in ϕ^4 theory*, [arXiv:hep-ph/9705268] Eur. Phys. J. C **2**, 569 (1998).
- [41] M. Hasenbusch, *A Monte Carlo study of the three-dimensional XY universality class: Universal amplitude ratios*, [arXiv:0810.2716], J. Stat. Mech. (2008) P12006.
- [42] M. Hasenbusch, *Variance-reduced estimator of the connected two-point function in the presence of a broken \mathbb{Z}_2 -symmetry*, [arXiv:1512.02491], Phys. Rev. E **93**, 032140 (2016).
- [43] M. Patra and M. Karttunen, *Stencils with Isotropic Discretization Error for Differential Operators*, Numerical Methods for Partial Differential Equations **22**, 936 (2006).
- [44] M. Hasenbusch, K. Pinn, and S. Vinti, *Critical Exponents of the 3D Ising Universality Class From Finite Size Scaling With Standard and Improved Actions*, [arXiv:hep-lat/9806012], Phys. Rev. B **59**, 11471 (1999).
- [45] <https://prng.di.unimi.it/>
- [46] D. Blackman and S. Vigna, *Scrambled Linear Pseudorandom Number Generators*, [arXiv:1805.01407], ACM Trans. Math. Softw. **47**, 36 (2021).
- [47] <https://www.pcg-random.org/posts/does-it-beat-the-minimal-standard.html>
- [48] [https://de.wikipedia.org/wiki/KISS_\(Zufallszahlengenerator\)](https://de.wikipedia.org/wiki/KISS_(Zufallszahlengenerator))
- [49] M. Saito and M. Matsumoto, “SIMD-oriented Fast Mersenne Twister: a 128-bit Pseudorandom Number Generator”, in *Monte Carlo and Quasi-Monte Carlo Methods 2006*, edited by A. Keller, S. Heinrich, H. Niederreiter, (Springer, 2008); M. Saito, Masters thesis, Math. Dept., Graduate School of science, Hiroshima University, 2007. The source code of the program is provided at <http://www.math.sci.hiroshima-u.ac.jp/~m-mat/MT/SFMT/index.html>
- [50] M. Hasenbusch, *ϕ^4 lattice model with cubic symmetry in three dimensions: Renormalization*

- group flow and first-order phase transitions*, [arXiv:2307.05165], Phys. Rev. B **109**, 054420 (2024).
- [51] P. Virtanen, R. Gommers, T. E. Oliphant et al., *SciPy 1.0–Fundamental Algorithms for Scientific Computing in Python*, [arXiv:1907.10121], Nature Methods **17**, 261 (2020).
- [52] J. D. Hunter, *Matplotlib: A 2D Graphics Environment*, Computing in Science & Engineering **9**, 90 (2007).
- [53] P. Hasenfratz and F. Niedermayer, *Perfect lattice action for asymptotically free theories*, [arXiv:hep-lat/9308004], Nucl. Phys. B **414**, 785 (1994).
- [54] M. Hasenbusch, *Finite size scaling study of lattice models in the three-dimensional Ising universality class*, [arXiv:1004.4486], Phys. Rev. B **82**, 174433 (2010).
- [55] M. Hasenbusch, *Monte Carlo study of a generalized icosahedral model on the simple cubic lattice*, [arXiv:2005.04448], Phys. Rev. B **102**, 024406 (2020).
- [56] M. Hasenbusch, *Three-dimensional $O(N)$ -invariant models at criticality for $N \geq 4$* , [arXiv:2112.03783], Phys. Rev. B **105**, 054428 (2022).
- [57] Martin Hasenbusch, Francesco Parisen Toldin, Andrea Pelissetto, and Ettore Vicari, *Universality class of 3D site-diluted and bond-diluted Ising systems*, [arXiv:cond-mat/0611707], J. Stat. Mech. (2007) P02016.
- [58] M. Hasenbusch, *Cubic fixed point in three dimensions: Monte Carlo simulations of the model on the simple cubic lattice*, [arXiv:2211.16170], Phys. Rev. B **107**, 024409 (2023).
- [59] K. G. Wilson and M. E. Fisher, *Critical exponents in 3.99 dimensions*, Phys. Rev. Lett. **28**, 240 (1972).
- [60] P. Butera and M. Comi, *N -vector spin models on the sc and the bcc lattices: a study of the critical behavior of the susceptibility and of the correlation length by high temperature series extended to order β^{21}* , [arXiv:hep-lat/9703018], Phys. Rev. B **56**, 8212 (1997).
- [61] Robert H. Swendsen, *Monte Carlo renormalization-group study of the $d = 3$ planar model*, Phys. Rev. B **27**, 391 (1983).
- [62] W. Janke, *Test of single cluster update for the three-dimensional XY model*, Phys. Lett. A **148**, 306 (1990).
- [63] M. Hasenbusch and T. Török, *High precision Monte Carlo study of the 3D XY-universality class*, [arXiv:cond-mat/9904408], J. Phys. A: Math. Gen. **32**, 6361 (1999).
- [64] A. Singasaas and G. Ahlers, *Universality of static properties near the superfluid transition in*

- ⁴ He, Phys. Rev. B **30**, 5103 (1984).
- [65] A. Oleaga, A. Salazar, D. Prabhakaran, J.G. Cheng, and J.S. Zhou, *Critical behavior of the paramagnetic to antiferromagnetic transition in orthorhombic and hexagonal phases of RMnO₃ (R=Sm, Tb, Dy, Ho, Er, Tm, Yb, Lu, Y)* Phys. Rev. B **85**, 184425 (2012).
- [66] A. Oleaga, A. Salazar, and Yu M. Bunkov, *3D-XY critical behavior of CsMnF₃ from static and dynamic thermal properties*, J. Phys.: Condens. Matter **26**, 096001 (2014).
- [67] M. V. Kompaniets and E. Panzer, *Minimally subtracted six-loop renormalization of ϕ^4 -symmetric theory and critical exponents*, [arXiv:1705.06483], Phys. Rev. D **96**, 036016 (2017).
- [68] O. Schnetz, Phys. Rev. D **97**, 085018 (2018); Maple package HyperlogProcedures, which is available on the Oliver Schnetz's homepage: <https://www.math.fau.de/person/oliver-schnetz/>
- [69] Abouzeid M. Shalaby, *Critical exponents of the $O(N)$ -symmetric ϕ^4 model from the ϵ^7 hypergeometric-Meijer resummation*, [arXiv:2005.12714], Eur. Phys. J. C **81**, 87 (2021).